HHS Public Access

Author manuscript

J Control Release. Author manuscript; available in PMC 2018 December 28.

Published in final edited form as:

J Control Release. 2017 December 28; 268: 147–158. doi:10.1016/j.jconrel.2017.10.020.

Exosome is a Mechanism of Intercellular Drug Transfer: Application of Quantitative Pharmacology

Jin Wang[1,2], **Bertrand Z. Yeung**[1,2,3], **Minjian Cui**[1,2,3], **Cody J. Peer**[4], **Ze Lu**[3], **William D. Figg**[4], **M. Guillaume Wientjes**[2,3], **Sukyung Woo**[1,6], and **Jessie L.-S. Au**[1,2,3,5,6]

[1]Department of Pharmaceutical Sciences, College of Pharmacy, University of Oklahoma Health Sciences Center, Oklahoma City, Oklahoma 73117, USA

[2]Institute of Quantitative Systems Pharmacology, Carlsbad, CA 92008, USA

[3]Optimum Therapeutics LLC, Carlsbad, CA 92008, USA

[4]Clinical Pharmacology Program, National Cancer Institute, NIH, Bethesda, MD 20892, USA

[5]College of Pharmacy, Taipei Medical University, Taipei, ROC

Abstract

Purpose—Exosomes are small membrane vesicles (30–100 nm in diameter) secreted by cells into extracellular space. The present study evaluated the effect of chemotherapeutic agents on exosome production and/or release, and quantified the contribution of exosomes to intercellular drug transfer and pharmacodynamics.

Methods—Human cancer cells (breast MCF7, breast-to-lung metastatic LM2, ovarian A2780 and OVCAR4) were treated with paclitaxel (PTX, 2–1000 nM) or doxorubicin (DOX, 20–1000 nM) for 24–48 h. Exosomes were isolated from the culture medium of drug-treated donor cells (Donor cells) using ultra-centrifugation, and analyzed for acetylcholinesterase activity, total proteins, drug concentrations, and biological effects (cytotoxicity and anti-migration) on drug-naïve recipient cells (Recipient cells). These results were used to develop computational predictive quantitative pharmacology models.

Results—Cells in exponential growth phase released ~220 exosomes/cell in culture medium. PTX and DOX significantly promoted exosome production and/or release in a dose- and time-dependent manner, with greater effects in ovarian cancer cells than in breast cancer cells. Exosomes isolated from Donor cells contained appreciable drug levels (2–7 pmole/10^6 cells after 24 h treatment with 100–1000 nM PTX), and caused cytotoxicity and inhibited migration of Recipient cells. Quantitative pharmacology models that integrated cellular PTX pharmacokinetics

[*]**Corresponding author:** Jessie L.S. Au, Pharm.D., Ph.D., Chief Scientific Officer, Optimum Therapeutics LLC, Founding Director, Institute of Quantitative Systems Pharmacology, Mosier Endowed Chair of Pharmaceutical Sciences, University of Oklahoma, Chair Professor of Systems Pharmacology, Taipei Medical University, Distinguished University Professor Emeritus, The Ohio State University, Address: 1815 Aston Ave. Suite 107. Carlsbad CA 92008, jau@optimumtx.com.

[6]Equal contribution

with PTX pharmacodynamics successfully predicted effects of exosomes on intercellular drug transfer, cytotoxicity of PTX on Donor cells and cytotoxicity of PTX-containing exosomes on Recipient cells. Additional model simulations indicate that within clinically achievable PTX concentrations, the contribution of exosomes to active drug efflux increased with drug concentration and exceeded the p-glycoprotein efflux when the latter was saturated.

Conclusions—Our results indicate (a) chemotherapeutic agents stimulate exosome production or release, and (b) exosome is a mechanism of intercellular drug transfer that contributes to pharmacodynamics of neighboring cells.

Graphical abstract

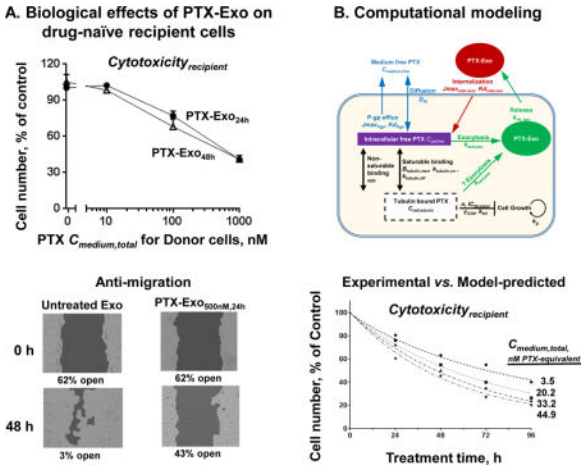

Keywords

exosome; exocytosis; intercellular drug transfer; quantitative pharmacology; chemoresistance

Introduction

Inadequate drug delivery is a major cause of treatment failures in solid tumors [1]. After entering the systemic circulation, e.g., *via* an intravenous injection, the drug encounters multiple transport barriers before reaching and exerting its action on the intended targets. Recent intraoperative intravital microscopy findings in patients further show that about one-half of vessels in human tumors are not patent or functional [2, 3]. These issues highlight the need to better understand the mechanisms of interstitial drug transfer. The present study examined the potential role of exosomes.

Cells utilize exocytosis to sort intracellular substances into exosomes that are subsequently released to the extracellular space [4]. Exosomes are small membrane vesicles with an average diameter of between 30 and 100 nm. They originate from the inward budding of endosomal lumen layer and carry cellular components including lipids, proteins (e.g., heat shock proteins, transcription factors, enzymes, major histocompatibility receptors and tetraspanins), and nuclei acids (e.g. DNA, mRNA, microRNA and long non-coding RNA) [4–7].

The life-cycle of exosomes comprises endosome biogenesis, trafficking, release, and re-uptake *via* endocytosis [4, 7, 8]. Biogenesis begins with internalization of plasma membrane as early endosomes, which later become multivesicular bodies and form intraluminal vesicles (pre-exosomes) that mature into exosomes. Contents of exosomes are sorted and loaded through ESCRT-dependent and -independent mechanisms. In the latter, a sphingolipid ceramide is involved in the loading of microRNA and lipid rafts into endosomes, and the initiation of exosome biogenesis [9, 10]. Several Rab proteins, including Rab-27a/b, Rab-11 and Rab-35, are known molecular motors that drive multivesicular bodies towards plasma membrane [11–13]. Release of exosomes into extracellular space is mediated by exocytosis, which involves fusion of exosome membrane with plasma membrane using SNARE (soluble N-ethylmaleimide sensitive fusion protein attachment receptors)-dependent and -independent mechanisms. Re-uptake of exosomes into cells primarily uses receptor-mediated endocytosis, with plasma membrane fusion and phagocytosis as minor pathways [6, 14].

Cancer cells generally produce higher levels of exosomes compared to normal cells [15]. Exosomes derived from cancer cells are involved in distal metastatic niche initiation [16, 17], intercellular communications (e.g., during drug resistance development [18, 19]), and immune system modulation [20, 21]. Cancer cells enhance their exosome secretion in response to environmental changes including pH [22], ion [23], temperature [24], and treatment by cytotoxic agents [25]. For example, liver HepG2 cells, when treated with cytotoxics (PTX, etoposide, irinotecan, carboplatin), release exosomes containing elevated level of heat shock proteins [25] triggered as a response to stress and as a survival mechanism [26].

Most exosome studies have focused on characterizing their contents and biological functions [13, 15–18, 27, 28]. The current study used *in vitro* experiments and *in silico* studies to investigate the intercellular drug transfer *via* exosomes and the quantitative relationship between this process and pharmacodynamics (PD) in solid tumors. Paclitaxel (PTX) and doxorubicin (DOX) were the test drugs as they are commonly used in first-line therapy of multiple types of major solid tumors including, e.g., ovarian, breast, lung, and prostate cancers [29]. Our results indicate exosomes is a mechanism of intercellular drug transfer with significant pharmacological consequences.

Materials and methods

Reagents

PTX and DOX (purity >99.5%), and cell culture grade dimethyl sulfoxide (DMSO) were purchased from Sigma-Aldrich (St. Louis, MO). Drug stock solutions were prepared in DMSO and diluted to desired concentrations such that the DMSO concentration was below 0.5%.

Cell culture

Human breast adenocarcinoma MCF7 cells were purchased from ATCC (Manassas, VA). LM2 cells, a highly breast-to-lung metastatic subline of human breast cancer MDA-MB-231

cells [30], were a gift from Dr. Y. Kang (Princeton University, NJ). Human ovarian cancer A2780 and OVCAR4 cells were provided by Dr. D. Dhanasekaran (University of Oklahoma Health Sciences Center, OK). MCF7 and LM2 cells were maintained in DMEM (Mediatech, VA), and A2780 and OVCAR4 cells in RPMI-1640 (ATCC). The medium for cell growth (Growth Medium) was supplemented with 10% fetal bovine serum (FBS, Atlanta Biologicals, GA), whereas the medium for exosome isolation (Conditioned Medium) was supplemented with 10% exosome-depleted-FBS (System Biosciences, CA). All medium contained 100 IU/mL penicillin and 100 μg/mL streptomycin (Mediatech, VA). Cells were cultured in a humidified incubator at 37°C with 5% CO_2.

Effects of PTX and DOX on exosomes

Effects of PTX and DOX on exosome production and release were studied using cytotoxic drug concentrations that produced 20, 50 and 80% of their maximal cytotoxicity (EC_{20}, EC_{50} and EC_{80}; see below for their determination). Exosomes collected from cells treated with drugs (Donor cells) are denoted as Drug-$Exo_{conc,time}$, e.g., PTX-$Exo_{500nM,24h}$ denotes exosomes from Donor cells treated with 500 nM PTX for 24 h. PTX-Exo was used to study its pharmacological effects ($Cytotoxicity_{recipient}$ and $Anti\text{-}migration_{recipient}$) on drug-naïve recipient cells (Recipient cells).

Exosome isolation, characterization, and quantification

Exosomes were isolated using a previously reported serial centrifugation protocol [31], with the following modifications. In brief, cells were cultured in T175 flasks, without or with drug. The post-incubation exosome-containing medium (Conditioned Medium) was collected at preselected time points, centrifuged twice, first at 2,000 × g for 10 min and then 10,000 × g for 30 min, to remove dead cells and debris. The supernatant was transferred and ultracentrifuged at 100,000 × g for 18 h at 4°C using a type 50.2 Ti rotor (Optima™ L-100 XP, Beckman Coulter Instruments). The pellet was washed once with 4 mL phosphate-buffered saline (PBS, pH 7.4), then ultra-centrifuged at 100,000 × g for 70 min at 4°C. For studying biological activity of exosomes, the resulting pellet was re-suspended in Growth Medium supplemented with 10% exosome-depleted FBS after PBS wash. For the remaining studies, the pellet was re-suspended in 150 μL PBS.

Exosome morphology was characterized using transmission electron microscopy. In brief, an exosome sample was diluted 1:100 in PBS, loaded on a 400 mesh, Formvar-coated, glow discharged copper grid using the single drop method. The liquid was removed 60–90 s later by wicking with filter paper and the exosome-loaded grid washed with deionized water for 10 s. After removing the water again with filter paper, the sample was stained with 4% uranyl acetate (pH 4.4, negative staining solution) for 60 s, washed in deionized water and air dried at room temperature. The grid was then viewed on a transmission electron microscope (Hitachi H7600, equipped with a 2k × 2k AMT digital camera) at 80 kV. A second aliquot of exosome suspension was used to determine exosome size using nanoparticle tracking analysis (NanoSight NS300; Malvern Instruments, Inc., UK). A third aliquot of exosome suspension was used to determine the total protein amount by BCA assay (Pierce kit, ThermoFisher Scientific Inc., CA). Another aliquot was used to determine the activity of acetylcholinesterase (AChE), an enzyme found in exosomes [12, 23], by the

Ellman colorimetric assay (Sigma-Aldrich) [32]. Briefly, exosome suspension (20 μL) was added to an aqueous reaction system (80 μL) containing 1 mM 5,5′-dithio-bis(2-nitrobenzoic acid) and 3 mM acetylthiocholine chloride (substrate for AChE), per well in a 96-well plate. After 40 min incubation at room temperature, the absorbance at 412 nm was determined using Synergy HT microplate reader (BioTek Instruments, VT). Standard curves of AChE activity were established using plasma exosome standards calibrated by NanoSight analysis (System BioSciences) and used to calculate the exosome quantity.

The levels of exosome protein markers TSG101 and CD63 were analyzed by Western blotting. Samples of exosomes or Donor cell lysates containing 60 μg proteins in RIPA lysis buffer (ThermoFisher Scientific) were mixed with a protease and phosphatase inhibitor cocktail (ThermoFisher Scientific), and the mixture was loaded on 10% Mini-PROTEAN® TGX pre-cast gel (BioRad Laboratories, CA). After electrophoresis, proteins were transferred to a 0.2 μm nitrocellulose membrane (BioRad Laboratories) and probed sequentially with primary antibodies (mouse IgG anti-CD63 and anti-TSG101 from Santa Cruz Biotechnology (Dallas, TX), rabbit IgG anti-beta actin and anti-calnexin from Cell Signaling Technology (Danvers, MA)), and then with fluorescent secondary antibodies (IRDye® 800CW goat anti-mouse and goat anti-rabbit, LI-COR Inc., NE). Fluorescence intensity was quantified using Odyssey CLx system (LI-COR Inc.).

Biological activities of PTX, DOX and PTX-Exo

We measured the cytotoxicity of PTX and DOX on donor cells ($Cytotoxicity_{donor}$) and the cytotoxicity of PTX-Exo on Recipient cells ($Cytotoxicity_{recipient}$) using the sulforhodamine B (SRB) colorimetric assay [33]. In brief, cells (5000 per 100 μL Growth Medium per well in 96-well plate) were seeded overnight, treated with drugs or PTX-Exo for 48 h, fixed with trichloroacetic acid (10% w/v, 100 μL per well, 30 min at 37°C) after removing the medium, washed gently with tap water three times, air-dried overnight, and stained with SRB (0.1% in 1% acetic acid (v/v), 100 μL per well, 30 min at room temperature) with gentle agitation. After removing the excess SRB by washing four times with 1% acetic acid, the cell-bound SRB was dissolved with Tris base solution (10 mM, 100 μL per well) and the absorbance measured at 510 nm using Synergy HT microplate reader. The concentration-effect relationships were analyzed with a sigmoidal Hill equation using nonlinear least square regression [34] (Prism 7, GraphPad Software, CA). For PTX, the Hill equation was modified with a residual unaffected fraction R_e as we previously described [34]. The analysis provided the drug concentration producing 20%, 50% and 80% of the maximal cytotoxicity (EC_{20}, EC_{50} and EC_{80}, respectively).

$Anti\text{-}migration_{recipient}$ was measured using the wound healing assay that measures cell migration [35]; the assay used serum-free medium to minimize cell proliferation. Results of pilot studies indicated only one of the four cell lines (LM2) remained viable in serum-free medium after 48 h and $PTX\text{-}Exo_{1000nM,24–48h}$ induced shrinkage and fragmentation in Recipient cells. Therefore, the study used LM2 cells as Recipient cells and $PTX\text{-}Exo_{5–500nM,24–48h}$. Briefly, cells were cultured in Growth Medium supplemented with 10% FBS on a tissue culture-coated (vacuum gas-plasma, hydrophilic and negative charge surface) 6-well plate (Corning Incorporated, NY) and allowed to grow to confluence, after

which time the medium was replaced with serum-free Growth Medium. The growth surface was scratched with a 200 μL pipet tip to create an open wound area, and cell debris was carefully washed off with pre-warmed DMEM. Afterwards, a suspension of exosomes (containing 100 μg proteins in 2 mL serum-free medium) was added to each well, and microscopic images of a fixed field were obtained before and after scratching (0 h, 24 h and 48 h). The open wound area was measured as fraction of area not covered by cells using TScratch, a stand-alone Matlab application that measures the covered pixels *vs.* the uncovered pixels of an image [36] with default detection threshold settings.

Quantification of PTX in PTX-Exo and cell lysates

Cells were treated with PTX for 24 h. PTX-Exo was collected from Conditioned Medium as described above. The remaining cells were washed with PBS and trypsinized, collected, and stained with trypan blue. The number of trypan blue-excluding cells were counted and lyzed with RIPA lysis buffer. Drug concentrations in PTX-Exo and cell lysates were measured using high performance liquid chromatography-tandem mass spectrometry (LC-MS/MS). First, PTX in the sample was extracted with 10x volume of methyl t-butyl ether containing 10 ng/mL of the internal standard docetaxel. The organic phase containing paclitaxel was separated, evaporated, and reconstituted with 10 μL of 0.1% aqueous formic acid/methanol (40/60, v/v). A calibration curve was performed using seven calibration standards covering a dynamic range of 1 – 1,000 ng/mL, prepared in the same biological matrix and run in duplicates. The best-fit line was obtained using linear regression with $1/x^2$ weighting. Quality control standards were prepared in quintuplet at each of three levels (low (3 ng/mL), mid (50 ng/mL), high (800 ng/mL)), and back-calculated against the best-fit line to ensure accuracy and precision of the assay.

For LC-MS/MS analysis, samples (10 μL) were injected onto a Symmetry Shield RP18 column (2.1×50 mm, 3.5 μm; Waters, MA), using a gradient elution scheme of 0.1% aqueous formic acid in methanol, where methanol was increased from 40% to 100% in 7 min before returning to 40% by the end of the 10 min run (flow rate 0.2 mL/min). The column eluent was directed into an electrospray ionization triple quadrupole mass spectrometer (Micromass Quattro Premier XE; Waters) for detection based on multiple reaction monitoring of a structural fragment in the positive ion mode. PTX was monitored by the mass transition from precursor ions to product ions of m/z 854.0➔287.0 (collision energy 16 V), and docetaxel by transition of m/z 806.8➔526.3 (collision energy 9 V). Universal mass spectrometer settings included capillary voltage of 3500 V, cone voltage of 25 V, source temperature 120°C, desolvation temperature 400°C, and desolvation gas flow (N2) of 600 L/hr.

Quantitative pharmacology modeling of exosome-mediated intercellular drug transfer and biological effects: Overview

The experimental results indicated exosomes collected from PTX-treated Donor cells contained high drug concentrations, served as a mechanism of intercellular transfer and conferred biological activities on drug-naïve Recipient cells. We established predictive quantitative pharmacology (QP) models to depict these processes, as follows. First, we modified our previously published PTX cellular pharmacokinetic (PK) models [37–39] to

include the sorting and release of exosomes and their re-uptake *via* receptor-mediated endocytosis. These models were used together with previously published model parameters and experimental results from the current study to obtain values of the exosome-related model parameters. The resulting equations plus parameter values were used to simulate the drug concentrations derived from PTX-Exo, in cells and medium. Next, we established PD models to depict the relationships between total extracellular/intracellular drug concentrations (including the pharmacologically active tubulin-bound moiety) and drug-induced cytotoxicity. Model simulations and data fitting (nonlinear least-squares algorithm) were performed using Matlab Simbiology (Release 2016a, Mathworks, MA).

Development of cellular PK models

We previously established cellular PTX PK models that have since been adopted by multiple investigator groups [34, 38–43]. The current study extended these earlier models to account for exosome-related processes. The model assumptions are (a) unbound drug in medium enters cells by passive diffusion, (b) saturable drug binding to proteins in extracellular fluid and to intracellular tubulin, plus non-saturable drug binding to other intracellular organelles, (c) drug efflux from cells uses a combination of passive diffusion, p-glycoprotein (Pgp)-mediated saturable efflux, and release of drug-containing exosomes, (d) first order sorting of intracellular unbound drug into exosomes through the endosomal transport system, (e) first order release of exosomes from the cell into extracellular space, and (f) internalization of drug-containing exosomes through saturable receptor-mediated endocytosis [14, 44]. The exosome-related processes in (c) through (f) are new, whereas the remaining processes describe the cross-membrane drug transportation and intracellular drug distribution as established previously [37–39]. To simplify the model, we assumed negligible PTX transfer between $C_{medium,free}$ and $C_{medium,exo}$.

The above processes are summarized in Figure 1. In general, subscripts are used to denote the various drug entities, their locations and transport mechanisms. For drug concentrations C, the first subscript indicates if the drug is located intracellularly or extracellularly (cell *vs.* medium) and the second subscript indicates if it is bound to proteins or exosomes, e.g., $C_{cell,tubulin}$ is tubulin-bound drug concentration in cells, and $C_{medium,exo}$ and $C_{cell,exo}$ are the respective drug concentrations in medium and cells derived from exosomes. Note that because $C_{medium,exo}$ and $C_{cell,exo}$ were calculated as amount divided by volume, $C_{medium,exo}$ does not equal $C_{cell,exo}$ due to difference in medium and cell volumes.

For transport, $Jmax$ is maximum rate and Kd denotes dissociation constant, and their subscript denotes the transport mechanism, e.g., $Jmax_{Pgp}$ is maximum Pgp-mediated efflux rate per cell and Kd_{Pgp} is dissociation constant of drug from Pgp, whereas $Jmax_{inter,exo}$ is maximum rate of receptor-mediated internalization of exosomes per cell and $Kd_{inter,exo}$ is dissociation constant of exosome bound to the receptor for internalization. $k_{sort,exo}$ and $k_{rel,exo}$ denote the rate constant for sorting and release of exosomes, respectively. For intracellular drug binding to its molecular target tubulin, $B_{tubulin,max}$ is the maximal available binding sites, and $k_{tubulin,on}$ and $k_{tubulin,off}$ are the respective association or disassociation rate constant. NSB is the proportionality constant for the linear nonsaturable drug binding in cells. D_{fd} is the diffusion rate constant of the free drug (i.e., unbound to

macromolecules) through cell membrane. V_{cell} and V_{medium} are volume of a single cell and extracellular medium, respectively. ICN and TCN are respectively the initial and total cell number, and were experimentally counted.

Eq. 1–2 depict $C_{cell,total}$ and $C_{medium,total}$ as sums of various intracellular and extracellular drug entities, respectively.

$$C_{cell,total}=C_{cell,free}+C_{cell,exo}+C_{cell,tubulin}+NSB\cdot C_{cell,free} \quad (1)$$

$$C_{medium,total}=C_{medium,free}+C_{medium,bound}+C_{medium,exo} \quad (2)$$

Eq. 3–5 describe the time-dependent changes of $C_{cell,free}$, $C_{cell,exo}$, and $C_{cell,tubulin}$. Based on the reported value of 0.99 ± 0.04 ligand per alpha/beta tubulin dimer [45, 46], we used a 1:1 PTX-tubulin binding stoichiometry (i.e., binding of $C_{cell,free}$ to tubulin increases linearly with $B_{tubulin,max}$). As reflected in these equations, there are three drug efflux mechanisms: passive diffusion (equals $D_{fd}\cdot C_{cell,free}$), and active efflux *via* Pgp (equals to ($Jmax_{Pgp}\cdot C_{cell,free}$)/($Kd_{Pgp}+C_{cell,free}$)) and exosomes (equals $k_{rel,exo}\cdot C_{cell,exo}\cdot V_{cell}$).

$$\begin{aligned}\frac{dC_{cell,free}}{dt}&=\frac{\left(D_{fd}\cdot C_{medium,free}-D_{fd}\cdot C_{cell,free}\frac{Jmax_{Pgp}\cdot C_{cell,free}}{Kd_{Pgp}+C_{cell,free}}+\frac{Jmax_{inter,exo}\cdot C_{medium,exo}}{Kd_{inter,exo}+C_{medium,exo}}\right)}{V_{cell}}\\&-k_{sort,exo}\cdot C_{cell,free}\\&+k_{tubulin,off}\cdot C_{cell,tubulin}\\&-k_{tubulin,on}\cdot C_{cell,free}\cdot(B_{tubulin,max}-C_{cell,tubulin})\end{aligned} \quad (3)$$

$$\frac{dC_{cell,exo}}{dt}=k_{sort,exo}\cdot C_{cell,free}-k_{rel,exo}\cdot C_{cell,exo} \quad (4)$$

$$\frac{dC_{cell,tubulin}}{dt}=k_{tubulin,on}\cdot C_{cell,free}\cdot(B_{tubulin,max}-C_{cell,tubulin})-k_{tubulin,off}\cdot C_{cell,tubulin} \quad (5)$$

We reported $B_{tubulin,max}$ increases linearly with time (from an initial value $B_{tubulin,initial}$) and the corresponding rate constant $kB_{tubulin,max}$ changes with drug concentration [39]; these kinetic processes are captured in Eq. 6 and 7. Eq. 7 was obtained by nonlinear regression of the plot of $kB_{tubulin,max}$ *vs.* $C_{cell,free}$ (r^2 = 0.998), where the experimental results were obtained from our earlier study [39].

$$\frac{B_{tubulin,\max}}{\mathrm{dt}} = B_{tubulin,initial} \cdot k_{Btubulin,max} \quad (6)$$

$$k_{Btubulin,max} = 408.48 \cdot C_{cell,free}{}^{0.2941} \quad (7)$$

Eq. 8–10 describe changes of $C_{medium,free}$, $C_{medium,exo}$, and $C_{medium,bound}$ with time, where $B_{medium,max}$ is maximum saturable drug binding sites in medium.

$$\frac{dC_{medium,free}}{dt} = \left(-D_{fd} \cdot C_{medium,free} + D_{fd} \cdot C_{cell,free} + \frac{J_{max,Pgp} \cdot C_{cell,free}}{Kd_{Pgp} + C_{cell,free}} \right) \cdot \frac{TCN}{V medium} \quad (8)$$

$$\frac{dC_{medium,exo}}{dt} = (k_{rel,exo} \cdot C_{cell,exo} \cdot V_{cell} - \frac{Jmax_{inter,exo} \cdot C_{medium,exo}}{Kd_{inter,exo} + C_{medium,exo}}) \cdot \frac{TCN}{V medium} \quad (9)$$

$$C_{medium,bound} = \frac{C_{medium,free} \cdot B_{medium,max}}{Kd_{medium,bound} + C_{medium,free}} \quad (10)$$

For initial conditions (before treatment), $C_{medium,exo}$ equals zero, and $C_{medium,free}$ and $C_{medium,bound}$ were calculated from $C_{medium,total}$ using Eq. 11 (obtained by substituting Eq. 10 into Eq. 2, followed by rearrangement).

$$C_{medium,free} = \frac{-(Kd_{medium,bound} + B_{medium,max} - C_{medium,total}) + \sqrt{(Kd_{medium,bound} + B_{medium,max} - C_{medium,total}) - 4 \cdot (C_{medium,t}}}{2}$$

(11)

Development of PD models

PD models describe cytotoxicity as a function of drug treatment (concentration and time). Eq. 12 depicts the net change in *TCN* due to (a) cell growth over time at a rate constant k_g until confluence, and (b) drug-induced cell kill as function of concentration of tubulin-bound drug. *TCNss* is maximal cell number at confluence. k_{kill} is maximum cell kill rate constant. Note that Eq. 12 does not account for potential concentration-dependent changes in k_{kill}. IC_{50} is tubulin-bound drug concentration that generates 50% maximum cell kill. n is the Hill exponent. In view of the time- and dose-dependent PTX cytotoxicity [34] and the development of drug resistance over time in MCF7 cells [47], we used Eq. 13 to depict the

time-dependent changes in IC_{50}, where $IC_{50,initial}$ is the IC_{50} value at time zero and γ_{IC50} is the rate of IC_{50} change per unit time t.

$$\frac{dTCN}{dt}=k_{growth}\cdot \mathrm{TCN}\cdot\left(1-\frac{TCN}{TCNss}\right)-k_{kill}\cdot\left(\frac{C_{cell,tubulin}{}^{n}}{C_{cell,tubulin}{}^{n}+IC_{50}^{n}}\right)\cdot TCN \quad (12)$$

$$IC_{50}=IC_{50,initial}+\gamma_{IC50}\cdot t \quad (13)$$

Model parameterization

The parameters for exosome-independent processes were obtained as follows. D_{fd}, and Kd_{Pgp} were taken from our published results [37, 39]. The calculation of PTX sequestration into exosomes required the $C_{cell,free}$-time profiles, which in turn required the rate constants of drug-tubulin interactions ($k_{tubulin,on}$, $k_{tubulin,off}$). PTX binding to tubulin depends on their nucleotide contents (GTP or GDP) and can be high affinity (Kd of 15 to 60 nM) or low affinity (Kd of 2 to 3 μM) [46, 48–51]. We used the reported parameters for high affinity binding ($k_{tubulin,on}$ of 2 $nM^{-1}s^{-1}$, $k_{tubulin,off}$ of 30 s^{-1}, Kd of 15 nM [48]). The current models also required $B_{tubulin,initial}$ and $kB_{tubulin}$, which were obtained in two-steps: we first modified Eq. 1 to 6 to remove the exosome-related components because drug binding to tubulin is independent of exosomes, and then we fitted the modified equations to our previously obtained experimental results ($C_{cell,total}$ *vs.* time plots after treatment with 0.1–1000 nM PTX [39]) to obtain the best-fitting parameters values.

To obtain the rate constants for the exosome-related PK processes (sorting, release, endocytosis), we used the above parameters together with the current models (Eq. 1–9 that incorporated exosome-related processes) to fit four sets of experimental data in PTX-treated Donor MCF7 cells obtained in our previous studies [27, 29], i.e., (a) $C_{cell,total}$ *vs.* time plots, (b) time-dependent depletion of $C_{medium,total}$ as function of initial $C_{medium,total}$ (1 to 1000 nM), (c) $Cytotoxicity_{donor}$ *vs.* treatment duration plots, and (d) ratio of $A_{medium,exo}$ [drug amount in exosomes in culture medium, equals $C_{medium,total}$ times V_{medium}] to $A_{cell,total}$ [drug amount in Donor cells, equals $C_{cell,total}$ times V_{cell} times TCN] at 24 h. The first three data sets were obtained from our earlier studies [34, 38, 39], whereas the last data set was from the current study (see Table 2 in Results). For example, $k_{sort,exo}$, $k_{rel,exo}$, $Jmax_{inter,exo}$, and $Kd_{inter,exo}$ were obtained by simultaneously fitting the plots (a), (b) and (d) (see Figures 5A, 5B and 5D in Results) with Eq. 1–5, Eq. 2 and 8–10, and Eq. 1 and 4, respectively.

PD parameters (k_{kill}, n, $IC_{50,initial}$, γ_{IC50}) were obtained using experimental results from our previous study [34] and the current study, by fitting Eq. 1–13 to the above plot (c) (see Figure 5C in Results). k_g was calculated from the cell doubling time [52]. TCN_{ss} was experimentally counted.

Evaluate model performance

QP models were used to predict the changes in $Cytotoxicity_{recipient}$ of PTX-Exo and $Cytotoxicity_{donor}$ of PTX due to exosome-mediated drug efflux. The model-predicted data

were then compared with experimental results to evaluate model performance. The deviation between model-predicted results and experimentally observed results, as percentage, was calculated using Eq. 14 where O_i is the observation value and P_i is the predicted value.

$$M = \frac{100}{n} \cdot \sum_{i=1}^{n} \left(\frac{O_i - P_i}{O_i} \right) \quad (14)$$

Sensitivity analysis

The four parameters on exosome-mediated drug transfer processes ($k_{sort,exo}$, $k_{rel,exo}$, $Jmax_{inter,exo}$, $Kd_{inter,exo}$) were evaluated for their effects on three cellular PK and PD endpoints ($C_{cell,total}$, $C_{cell,tubulin}$, $Cytotoxicity$) in both Donor and Recipient cells. Sensitivity analysis was performed by (a) changing the value (10-fold increase or decrease) of a selected parameter while keeping all other parameters constant in Donor cells, and (b) comparing the differences in the simulated outcomes without or with the parameter value change. These exosome-related effects were further compared to the effects caused by changes in tubulin binding capacity, a parameter we have demonstrated to significantly alter the cellular PTX PK [37, 39]. Simulations of $Cytotoxicity_{recipient}$ of PTX-Exo used equal cell numbers, i.e., PTX-Exo derived from a selected number of Donor cells were applied to the same number of Recipient cells.

Statistical analysis

Experimental results were analyzed for statistical significance using Student's t-test (unpaired, two-tailed) or Dunnett's test (Prism 7). $p<0.05$ was considered as significant. Data are presented as mean ± SD (standard deviation) or mean ± SEM (standard error of the mean).

Results

Characterization of exosomes

Transmission electron microscopy (Figure 2A) showed the spherical shape of exosomes (from MCF7 cells) obtained after drying and processing. The average particle diameter, based on nanoparticle tracking analysis, was 108 nm (n=100, Figure 2B). Exosomes contained high levels of CD63 (a tetraspanin and marker of exosomes) and TSG101 (a component of ESCRT-I complex or endosomal sorting complexes required for transport), but undetectable levels of skeleton protein β-actin and endoplasmic reticulum protein calnexin, whereas the reverse was found for Donor cell lysates (Figure 2C).

$Cytotoxicity_{donor}$ of PTX and DOX

Figure 3A shows $Cytotoxicity_{donor}$ of PTX and DOX. PTX yielded incomplete cytotoxicity in all 4 cells; MCF7 cells were the least sensitive with the highest residual unaffected fraction R_e. In contrast, DOX yielded complete cytotoxicity in the two cells studied, with ~8-times higher activity in A2780 cells compared to MCF7 cells. Subsequent studies on the

effects of PTX and DOX on exosomes used drug concentrations that corresponded to their EC_{20}, EC_{50}, and EC_{80} values in individual cell lines.

PTX and DOX stimulated exosome production and/or release

Figure 3B shows the levels of exosomes in Conditioned Medium. Without drug treatments, the four cells during exponential growth phase (over 24 to 48 h) yielded comparable exosome levels, ranging from 170 ± 35 to 280 ± 68 exosomes per cell (mean ± SEM). Treatments with cytotoxic concentrations of PTX or DOX generally enhanced the exosome levels, in drug concentration- and time-dependent manners. The data also showed drug- and cell-specific differences. For example, compared to untreated control, treatments with PTX at EC_{80} for 48 h increased the exosome level by ~3-folds in the two breast cells (LM2 and MCF7) and ~10-folds in the two ovarian cells (A2780 and OVCAR4), and the exosome level in MCF7 and A2780 cells continued to increase with time (50–200% higher after 48 h treatment compared to 24 h) whereas the maximal increase was reached at 24 h with no further increases in LM2 or OVCAR4 cells. Similarly, treatment with DOX at EC_{80} enhanced the exosome level in MCF7 by 4- to 6-folds after 24 or 48 h, but required longer treatment duration to produce changes in A2780 cells (no change after 24 h and 7-fold increase after 48 h).

Quantification of PTX in PTX-Exo and cell lysate by LC-MS/MS

Table 1 summarizes the LC-MS/MS results of PTX concentrations or amounts in PTX-Exo or cell lysates, after 24 h treatment. In general, the four cancer cells showed comparable PTX concentrations in cell lysates or exosomes (e.g., ~27 pmole in lysates and ~1.5 pmole in exosomes per 10^6 trypan blue-excluding cells at 100 nM $C_{medium,total}$), and increasing PTX concentrations/amounts with increasing $C_{medium,total}$. However, the ratios of PTX concentration in PTX-Exo and cell lysate indicate (a) substantial cell-specific differences, i.e., up to two-fold difference between cells (e.g., 4.3% in LM2 cells *vs.* 8.3% in OVCAR4 cells at 100 nM $C_{medium,total}$) and (b) nonlinear uptake of PTX and nonlinear drug sorting into PTX-Exo (e.g., the PTX concentration increases in PTX-Exo and cell lysate were not proportional to either the increase in $C_{medium,total}$ (average of ~4-folds *vs.* 10 folds) or to each other (e.g., average of ~2.5-folds *vs.* ~4-folds)).

The amount of PTX in PTX-Exo was between 6–10% of the amount in Donor cell lysate (Table 1). We further calculated the PTX concentration in PTX-Exo from MCF7 cells treated with 100 nM $C_{medium,total}$ for 24 h, as [$Amount_{medium,exo}$ of 1.6 pmole per 10^6 cells] divided by [Volume of exosomes excreted by 10^6 cells, calculated using an average exosome radius of 54 nm and release of 10^3 exosomes per cell (see Table 1)]; the resulting concentration in exosomes equaled 2.4 mM, which is ~60-times the $C_{cell,total}$ and ~30,000-times the $C_{medium,total}$ (experimentally determined to be 39 μM and 83 nM, respectively, after treatment with 100 nM for 24 h [39]).

PTX-Exo exhibited $Cytotoxicity_{recipient}$ and $Anti\text{-}migration_{recipient}$

Figure 4A compares the $Cytotoxicity_{recipient}$ of PTX to that of PTX-Exo. Each treatment condition had its own control, i.e., no drug for the PTX treatment and exosomes collected from untreated cells (Untreated-Exo) for the PTX-Exo treatment. The amount of PTX-Exo

added was calculated based on the drug concentration in PTX-Exo as determined by LC-MS/MS, whereas the amount of Untreated-Exo added was calculated to contain the same protein amount as in PTX-Exo. No cytotoxicity was observed in all control groups, confirming Untreated-Exo had no cytotoxicity (not shown). In contrast, PTX-$Exo_{10–1000nM,24–48h}$ induced significant $Cytotoxicity_{recipient}$ in all four cells; the extent increased with the drug treatment concentration and duration of Donor cells (e.g., greater cytotoxicity for PTX-Exo_{48h} compared to PTX-Exo_{24h}) and followed the rank order of the chemosensitivity of individual cells (LM2>MCF7>A2780>OVCAR4).

We further compared $Cytotoxicity_{recipient}$ of PTX and PTX-Exo, at equal PTX-equivalent concentrations (Figure 4B); the overlapping concentration-effect relationships of PTX and PTX-Exo in all 4 cells indicate $Cytotoxicity_{recipient}$ of PTX-Exo was due to its PTX content.

Figure 4C shows $Anti\text{-}migration_{recipient}$ of PTX-Exo. After 48 h incubation, the untreated control showed a much smaller scratch-induced open-wound gap (from 62% to 9%, equivalent to 85% reduction), indicating substantial cell migration. In comparison, Untreated-Exo slightly but significantly promoted the cell migration as indicated by a yet smaller open-wound gap (>90% reduction, $p<0.05$ compared to untreated control); this minor effect is consistent with the reported invasion and pre-metastasis functions of tumor-derived exosomes [16, 53]. In contrast, PTX-$Exo_{5–500nM,24–48h}$ significantly inhibited the migration, as indicated by a larger open wound area (e.g., decreased from 62% to 43%, equivalent to 31% reduction, for PTX-$Exo_{500nM,48h}$). As observed for $Cytotoxicity_{recipient}$, $Anti\text{-}migration_{recipient}$ of PTX-Exo generally increased with PTX treatment concentration and duration of Donor cells (Figure 4D); the differences between $C_{medium,total}$ of 5, 50 and 500 nM were significant ($p<0.05$ compared to untreated control or Untreated-Exo groups). However, prolonging treatment from 24 to 48 h yielded a significant difference only at the lowest concentration and not at the two higher concentrations; this concentration-dependence may be due to the different rates for $C_{exo,total}$ to equilibrate with $C_{cell,total}$.

Quantitative pharmacology models of exosome-mediated effects

Computational models were constructed to capture the above cellular PK and PD findings (Eq. 1–13). Figures 5A–5D show the best-fitting curves for changes in $C_{cell,total}$ over time at different initial $C_{medium,total}$, depletion of $C_{medium,total}$ as function of initial $C_{medium,total}$, $Cytotoxicity_{donor}$ as function of drug treatment duration and initial $C_{medium,total}$, and changes in % of $A_{medium,exo}$ as a fraction of $A_{cell,total}$ with treatment time at initial $C_{medium,total}$ of 100 and 1000 nM, respectively. Table 2 summarizes the best-fitting PK and PD model parameter values. The coefficients of variations (CV) for most parameters were between <10% to 25%; the three exceptions are the parameters for exosome transport $Kd_{inter,exo}$ and $k_{sort,exo}$ and for resistance development over time γ_{IC50} where the CV was between 45% and 67%; these high CV were in part due to the inability to experimentally measure $C_{cell,exo}$.

Comparisons of model parameter values provided the following insights regarding exosome-mediated drug transfer and PD. The value of $k_{sort,exo}$ of ~31 h^{-1} corresponds to a half-life of <2 min, indicating rapid sorting of $C_{cell,free}$ into exosomes. Internalization of PTX-Exo into Recipient cells was also rapid, as demonstrated by a relative high $Jmax_{inter,exo}$ value. In comparison, the release of PTX-Exo into extracellular medium was much slower ($k_{rel,exo}$ of

0.105 h^{-1} per cell, which corresponds to a half-life of ~6–7 h). Hence, release of PTX-Exo from Donor cells is rate-limiting for their appearance in extracellular fluid and Recipient cells. With respect to PD, the γ_{IC50} of 7.2 nM per h indicates a doubling of the initial IC_{50} of 826 nM in about 115 h, which is consistent with the finding of a separate study showing that continuous PTX treatment led to a 2-fold higher IC_{50} in human prostate PC3 cells after 120 h (unpublished results).

Evaluation of model performance

Figure 6 compares the QP model-simulated $Cytotoxicity_{recipient}$ of PTX-Exo with the experimental results, at four initial $C_{medum,exo}$ (3.5 to 45 nM) and four treatment durations (24 to 96 h). The good agreement between these results (average deviation of <10% for all data, <15% deviations for individual data points) indicates the QP models in Eq. 1–13 successfully depicted the pharmacological activity of PTX-Exo.

Sensitivity analysis

The sensitivity analysis results identified the different key determinants of three PK and PD endpoints ($C_{cell,total}$, $C_{cell,tubulin}$ and $Cytotoxicity$) in Donor and Recipient cells; these endpoints are expressed as area-under-curve from 0 to 24 h (Table 3). The three model parameters ($k_{sort,exo}$, $k_{rel,exo}$, $Jmax_{inter,exo}$) exerted different effects at low and high initial $C_{medium,total}$ (1 *vs.* 1000 nM) and in Donor *vs.* Recipient cells, as follows.

For Donor cells treated with 1 nM $C_{medium,total}$, a 10-fold increase or decrease in $k_{rel,exo}$ produced small-to-moderate changes in $C_{cell,total}$ (20–50%) and $C_{cell,tubulin}$ (51–100%), but significantly greater changes in $Cytotoxicity_{donor}$ (241%), whereas similar changes in $k_{sort,exo}$ or $Jmax_{inter,exo}$ yielded minor or no changes in all three endpoints (<20%). At 1000 nM $C_{medium,total}$ or when drug binding to tubulin would be saturated and consequently maximal cytotoxicity would have been reached, 10-fold changes in $k_{sort,exo}$ or $k_{rel,exo}$ produced 20–50% changes in $C_{cell,total}$ and/or $C_{cell,tubulin}$, whereas $Jmax_{inter,exo}$ had little or no effects, and none of the three parameters affected $Cytotoxicity_{donor}$. These findings indicate (a) exosome release played a greater role on $C_{cell,tubulin}$ and $C_{cell,total}$ compared to exosome sorting or re-uptake, especially at low $C_{medium,total}$ of 1 nM, and (b) exosome release played a major role in $Cytotoxicity_{donor}$ at low $C_{medium,total}$ but had no effect at high $C_{medium,total}$. These concentration-dependent outcomes indicate complex interplay between exosome-mediated processes and other competing linear and nonlinear processes that also determine $C_{cell,tubulin}$ and hence $Cytotoxicity_{donor}$.

Recipient cells showed changes in the opposite direction with substantial quantitative differences. Because <10% $C_{cell,total}$ in Donor cells was released in PTX-Exo, which was the drug source for Recipient cells, $C_{cell,total}$ in Recipient cells was much lower compared to Donor cells. In general, changes in exosome-related model parameters had greater effects on $Cytotoxicity_{recipient}$ than on $Cytotoxicity_{donor}$, especially at the high $C_{medium,total}$ of 1000 nM. Changes in $Jmax_{inter,exo}$ also affected $C_{cell,total}$ and $C_{cell,tubulin}$ in Recipient cells more than in Donor cells.

We further compared the effect of exocytosis of PTX-Exo to the effect of a known paclitaxel resistance mechanism, i.e., tubulin alteration resulting in reduced drug binding as reflected

by a lower $B_{tubulin,initial}$ [39, 54]. The simulation results indicate a 10-fold increase in $k_{rel,exo}$ yielded effects that are comparable to a 2-fold decrease in $B_{tubulin,initial}$ on all three endpoints in Donor cells. Changes in $B_{tubulin,initial}$ had less impact on Recipient cells compared to Donor cells, presumably due to nonlinear exocytosis and endocytosis of PTX-Exo.

Comparison of drug efflux rates by different mechanisms

We used simulations to compare the drug efflux rates *via* passive diffusion and the two active efflux by Pgp and exosomes; the simulations were for cells treated with PTX $C_{medium,total}$ of 0.1–1000 nM for 24 h or after $C_{cell,total}$ has reached a plateau level. The results, shown in Figure 7, indicate passive diffusion was the dominant efflux mechanism at all $C_{medium,total}$, accounting for at least 92% of total efflux. At $C_{medium,total}$ exceeding 30 nM or when PTX binding to tubulin was saturated, $C_{cell,free}$ increased nonlinearly with $C_{medium,total}$ and resulted in greater efflux by all three mechanisms such that efflux by passive diffusion increased from ~12-times to 44-times the active efflux at 1000 nM. The contributions of two active efflux mechanisms changed with $C_{medium,total}$ due to saturation of Pgp-efflux, i.e., Pgp-efflux initially exceeded exosome-efflux (e.g., 235%–88% higher at up to 100 nM $C_{medium,total}$) but became less efficient at higher $C_{medium,total}$ (e.g., one-fourth the exosome-efflux at 1000 nM).

Discussion

The present study indicated several new findings regarding the potential roles for exosomes in pharmacological effects of cytotoxics in solid tumors.

We observed that cytotoxics such as DOX and PTX stimulated the production and/or release of exosomes containing high drug levels. The sorting of intracellular drug content into exosomes and their release allows the cell to reduce the intracellular drug concentration (e.g., 15–50% reduction of $C_{cell,tubulin}$ in the current study). Hence, drug-stimulated exosome production/release may reduce drug activity, rendering this effect a potential new chemoresistance mechanism. This is supported by our QP model-simulated results indicating that in PTX treatments, a 10-fold increase in $k_{rel,exo}$ was as effective in reducing $Cytotoxicity_{donor}$ as a 2-fold reduction in drug binding to tubulin, a known mechanism of PTX resistance [54]. Note the current study was conducted using MCF7 cells which have relatively low Pgp level; under this setting the exosome-efflux accounted for up to 80% of total active drug efflux at initial $C_{medium,total}$ of 1000 nM, whereas Pgp-efflux accounted for the remaining 20%. It is conceivable that drug elimination *via* exosomes may become less pronounced in cells with higher Pgp levels. Studies to investigate the relative contribution of exosome- and Pgp-mediated drug depletion in cells with different Pgp expression are ongoing in our laboratory.

Second, we calculated the drug concentration in PTX-Exo per unit volume (i.e., 2.4 mM in PTX-Exo from MCF7 cells treated with 100 nM $C_{medium,total}$) was 60-times the $C_{cell,total}$ and 30,000-times the $C_{medium,total}$, indicating PTX-Exo represents an important drug depot. This high PTX level in exosomes is not likely due to pH trapping in acidic exosomes as reported for weakly basic drugs such as DOX and cisplatin [55–57], since the pKa of

paclitaxel is 11.5 and is unionized at physiological pH [58]. A possible cause is exosomes contain tubulin [59, 60], which, based on the extensive PTX binding to tubulin and the following calculation, would readily account for the high drug concentration in PTX-Exo. Based on our previously reported $C_{cell,total}$ of 39 μM at 100 nM $C_{medium,total}$ [39] and cell volume of 2 μL per 10^6 cells [39], and since nearly all $C_{cell,total}$ is due to macromolecule-bound drug, we calculated the maximal bound drug would be 78 pmole PTX per 10^6 cells. With tubulin being the primary binding site and because tubulins constitute ~1% of total proteins in neuroblastoma and HeLa cells (3 *vs.* 300 pg per cell [61]), the amount of tubulin-bound PTX would be 26 μmol per gram tubulin (equals 78 pmole divided by 3×10^6 pg). Using the experimentally determined protein amount in PTX-Exo (1.3 μg per 10^6 MCF7 cells) and assuming the same 1% protein-to-tubulin ratio as in cells, the tubulin amount in PTX-Exo would be 13 ng per 10^6 MCF7 cells, corresponding to a maximal tubulin-bound drug concentration of ~3.4 mM in PTX-Exo. This calculation shows that preferential sorting of tubulin and tubulin-bound PTX would lead to the high drug concentration in PTX-Exo observed in the present case. We further evaluated whether inclusion of this process (i.e., sorting of tubulin-bound drug into exosomes) in the QP model would significantly alter the PK/PD in Donor cells; the simulations indicated the model modification yielded negligible changes in the $C_{cell,total}$-time profiles (~5% compared to without this additional sorting step).

Third, our results indicate exosome is a mechanism of intercellular drug transfer. Unlike diffusion which is driven by the concentration gradient, exosomes, which use receptor-mediated endocytosis for internalization [14], enable the drug sequestered in exosomes to enter cells irrespective of the concentration gradient. An earlier study shows that exosomes isolated from prostate cancer cells and loaded with PTX extracellularly enter cells *via* endocytosis [62]. Another notable property is that exosomes, as nanoparticles, are less readily removed from tumor interstitium compared to free drug and thereby provide sustained drug exposure in tumors. This property may have therapeutic importance as our experimental results indicate substantial $Cytotoxicity_{recipient}$ by PTX-Exo.

Fourth, our study used PTX-Exo collected from epithelial cancer cells. Their pharmacological effects, together with an earlier report that PTX-treated dendritic cells yielded exosomes capable of inducing cytotoxicity in *mdr1*-transfected canine kidney cells [63], suggest release of pharmacologically active PTX-Exo is a general property that occurs in different cell types/lineages.

Fifth, the finding that exosome release, rather than sorting or internalization *via* receptor-mediated endocytosis, is the rate-limiting step of exosome appearance in Recipient cells suggests that its perturbation, e.g., by agents that block exosome release, will be a critical determinant of intercellular drug transfer.

Finally, the current study established the utility of QP models to delineate the complex interplay between exosome-related processes and other competing intracellular and extracellular processes, and the pharmacological consequences of these various processes. The current, first-generation model does not account for cell doubling leading to dilution of drug concentration, concentration-dependent cell kill mechanisms (e.g., apoptosis, necrosis),

potential cytostasis (which would decrease the k_{growth}), nor PTX transfer between $C_{medium,free}$ and $C_{medium,exo}$. Such dynamic changes may be considered in future model development. Additional areas that warrant further studies include spatial distribution and residence of exosomes within tumor interstitium, their transport into systemic circulation, and factors that alter their production and release.

Conclusion

The present study demonstrated exosomes as a mechanism to reduce intracellular drug concentration as well as a mechanism of intercellular drug transfer, with significant pharmacological consequences. We further provided the first QP models that (a) captured the PK of cellular PTX processing and drug release through exosomes, and (b) successfully described the effects of exosome exocytosis on PD in Donor cells and drug-naïve Recipient cells. These findings and computational tools may be used to interrogate exosomes as a resistance mechanism and as a means to deliver drugs to the hard-to-reach regions in solid tumors, and to predict the contributions of these opposite effects of exosomes to therapeutic outcomes.

Acknowledgments

Supported in part by research grants R01CA158300 (MGW, JLA), R01CA163015 (MGW, JLA), R01GM100487 (JLA, MGW) and R01EB015253 (JLA, MGW), from National Cancer Institute, National Institute of General Medical Sciences, and National Institute of Biomedical Imaging and Bioengineering, NIH, DHHS, and by RSG-16-006-01-CCE (SW) from American Cancer Society. Authors grateful acknowledge the assistance of Imaging Core Facility at Oklahoma Medical Research Foundation.

Abbreviations

AChE
acetylcholinesterase

Conditioned Medium
culture medium collected after incubating cells under preselected conditions

CV
coefficient of variation

$Cytotoxicity_{donor}$
cytotoxicity in Donor cells

$Cytotoxicity_{recipient}$
cytotoxicity in Recipient cells

DMSO
dimethyl sulfoxide

Donor cells
cells that provide drug-containing exosomes

DOX

doxorubicin

Drug-Exo$_{conc,time}$
exosomes collected from Donor cells treated with a drug at a preselected concentration for a preselected duration

E_{max}
maximum effect

ECn
drug concentration producing n% of E_{max}

ESCRT
endosomal sorting complexes required for transport

Growth Medium
cell culture medium supplemented with 10% fetal bovine serum (either unaltered or exosome-depleted) and antibiotics

IC_{50}
tubulin-bound paclitaxel concentration that generates 50% maximum cell kill

LC-MS/MS
liquid chromatography–tandem mass spectrometry

PBS
phosphate-buffered saline

PD
pharmacodynamics

Pgp
P-glycoprotein

PK
pharmacokinetics

PTX
paclitaxel

QP
quantitative pharmacology

Recipient cells
drug-naïve cells receiving treatment with drug-containing exosomes

SD
standard deviations

SEM

standard error of the mean

SRB
sulforhodamine B

A	denotes drug amount
B	denotes drug binding sites
C	denotes concentration
D	denotes diffusion
J	denotes flux
Kd	denotes dissociation constant
k	denotes rate constant
NSB	denotes non-saturable binding
t	denotes time
	subscripts are used to denote location (extracellular, intracellular, exosomes), drug moieties with respect to binding status (free, bound, total) to macromolecules/organelles (tubulin, exosomes)

References

1. Au JL, Yeung BZ, Wientjes MG, Lu Z, Wientjes MG. Delivery of cancer therapeutics to extracellular and intracellular targets: Determinants, barriers, challenges and opportunities. Adv Drug Deliv Rev. 2016; 97:280–301. [PubMed: 26686425]
2. Weis SM, Cheresh DA. Tumor angiogenesis: molecular pathways and therapeutic targets. Nat Med. 2011; 17:1359–1370. [PubMed: 22064426]
3. Fisher DT, Muhitch JB, Kim M, Doyen KC, Bogner PN, Evans SS, Skitzki JJ. Intraoperative intravital microscopy permits the study of human tumour vessels. Nat Commun. 2016; 7:10684. [PubMed: 26883450]
4. Raposo G, Stoorvogel W. Extracellular vesicles: exosomes, microvesicles, and friends. J Cell Biol. 2013; 200:373–383. [PubMed: 23420871]
5. Milane L, Singh A, Mattheolabakis G, Suresh M, Amiji MM. Exosome mediated communication within the tumor microenvironment. J Control Release. 2015; 219:278–294. [PubMed: 26143224]
6. Colombo M, Raposo G, Thery C. Biogenesis, secretion, and intercellular interactions of exosomes and other extracellular vesicles. Annu Rev Cell Dev Biol. 2014; 30:255–289. [PubMed: 25288114]
7. Camussi G, Deregibus MC, Bruno S, Cantaluppi V, Biancone L. Exosomes/microvesicles as a mechanism of cell-to-cell communication. Kidney Int. 2010; 78:838–848. [PubMed: 20703216]
8. Gyorgy B, Szabo TG, Pasztoi M, Pal Z, Misjak P, Aradi B, Laszlo V, Pallinger E, Pap E, Kittel A, Nagy G, Falus A, Buzas EI. Membrane vesicles, current state-of-the-art: emerging role of extracellular vesicles. Cell Mol Life Sci. 2011; 68:2667–2688. [PubMed: 21560073]
9. Hu Y, Yan C, Mu L, Huang K, Li X, Tao D, Wu Y, Qin J. Fibroblast-Derived Exosomes Contribute to Chemoresistance through Priming Cancer Stem Cells in Colorectal Cancer. PloS one. 2015; 10:e0125625. [PubMed: 25938772]
10. Trajkovic K, Hsu C, Chiantia S, Rajendran L, Wenzel D, Wieland F, Schwille P, Brugger B, Simons M. Ceramide triggers budding of exosome vesicles into multivesicular endosomes. Science. 2008; 319:1244–1247. [PubMed: 18309083]

11. Woodman PG. Biogenesis of the sorting endosome: the role of Rab5. Traffic. 2000; 1:695–701. [PubMed: 11208157]
12. Savina A, Vidal M, Colombo MI. The exosome pathway in K562 cells is regulated by Rab11. J Cell Sci. 2002; 115:2505–2515. [PubMed: 12045221]
13. Kosaka N, Iguchi H, Yoshioka Y, Takeshita F, Matsuki Y, Ochiya T. Secretory mechanisms and intercellular transfer of microRNAs in living cells. J Bio Chem. 2010; 285:17442–17452. [PubMed: 20353945]
14. Christianson HC, Svensson KJ, van Kuppevelt TH, Li JP, Belting M. Cancer cell exosomes depend on cell-surface heparan sulfate proteoglycans for their internalization and functional activity. Proc Natl Acad Sci U S A. 2013; 110:17380–17385. [PubMed: 24101524]
15. Logozzi M, De Milito A, Lugini L, Borghi M, Calabro L, Spada M, Perdicchio M, Marino ML, Federici C, Iessi E, Brambilla D, Venturi G, Lozupone F, Santinami M, Huber V, Maio M, Rivoltini L, Fais S. High levels of exosomes expressing CD63 and caveolin-1 in plasma of melanoma patients. PLoS One. 2009; 4:e5219. [PubMed: 19381331]
16. Costa-Silva B, Aiello NM, Ocean AJ, Singh S, Zhang H, Thakur BK, Becker A, Hoshino A, Mark MT, Molina H, Xiang J, Zhang T, Theilen TM, Garcia-Santos G, Williams C, Ararso Y, Huang Y, Rodrigues G, Shen TL, Labori KJ, Lothe IM, Kure EH, Hernandez J, Doussot A, Ebbesen SH, Grandgenett PM, Hollingsworth MA, Jain M, Mallya K, Batra SK, Jarnagin WR, Schwartz RE, Matei I, Peinado H, Stanger BZ, Bromberg J, Lyden D. Pancreatic cancer exosomes initiate pre-metastatic niche formation in the liver. Nat Cell Biol. 2015; 17:816–826. [PubMed: 25985394]
17. Melo SA, Sugimoto H, O'Connell JT, Kato N, Villanueva A, Vidal A, Qiu L, Vitkin E, Perelman LT, Melo CA, Lucci A, Ivan C, Calin GA, Kalluri R. Cancer exosomes perform cell-independent microRNA biogenesis and promote tumorigenesis. Cancer Cell. 2014; 26:707–721. [PubMed: 25446899]
18. Qu L, Ding J, Chen C, Wu ZJ, Liu B, Gao Y, Chen W, Liu F, Sun W, Li XF, Wang X, Wang Y, Xu ZY, Gao L, Yang Q, Xu B, Li YM, Fang ZY, Xu ZP, Bao Y, Wu DS, Miao X, Sun HY, Sun YH, Wang HY, Wang LH. Exosome-Transmitted lncARSR Promotes Sunitinib Resistance in Renal Cancer by Acting as a Competing Endogenous RNA. Cancer Cell. 2016; 29:653–668. [PubMed: 27117758]
19. Stone L. Kidney cancer: Exosome transmission of sunitinib resistance. Nat Rev Urol. 2016; 13:297. [PubMed: 27162048]
20. Muller L, Mitsuhashi M, Simms P, Gooding WE, Whiteside TL. Tumor-derived exosomes regulate expression of immune function-related genes in human T cell subsets. Sci Rep. 2016; 6:20254. [PubMed: 26842680]
21. Robbins PD, Morelli AE. Regulation of immune responses by extracellular vesicles. Nat Rev Immunol. 2014; 14:195–208. [PubMed: 24566916]
22. Parolini I, Federici C, Raggi C, Lugini L, Palleschi S, De Milito A, Coscia C, Iessi E, Logozzi M, Molinari A, Colone M, Tatti M, Sargiacomo M, Fais S. Microenvironmental pH is a key factor for exosome traffic in tumor cells. J Bio Chem. 2009; 284:34211–34222. [PubMed: 19801663]
23. Savina A, Furlan M, Vidal M, Colombo MI. Exosome release is regulated by a calcium-dependent mechanism in K562 cells. J Bio Chem. 2003; 278:20083–20090. [PubMed: 12639953]
24. Yang Y, Chen Y, Zhang F, Zhao Q, Zhong H. Increased anti-tumour activity by exosomes derived from doxorubicin-treated tumour cells via heat stress. International journal of hyperthermia : the official journal of European Society for Hyperthermic Oncology, North American Hyperthermia Group. 2015; 31:498–506.
25. Lv LH, Wan YL, Lin Y, Zhang W, Yang M, Li GL, Lin HM, Shang CZ, Chen YJ, Min J. Anticancer drugs cause release of exosomes with heat shock proteins from human hepatocellular carcinoma cells that elicit effective natural killer cell antitumor responses in vitro. J Bio Chem. 2012; 287:15874–15885. [PubMed: 22396543]
26. Walter S, Buchner J. Molecular chaperones–cellular machines for protein folding. Angew Chem Int Ed Engl. 2002; 41:1098–1113. [PubMed: 12491239]
27. Chalmin F, Ladoire S, Mignot G, Vincent J, Bruchard M, Remy-Martin JP, Boireau W, Rouleau A, Simon B, Lanneau D, Thonel A De, Hamman G, Multhoff A, Martin F, Chauffert B, Solary E, Zitvogel L, Garrido C, Ryffel B, Borg C, Apetoh L, Rebe C, Ghiringhelli F. Membrane-associated

Hsp72 from tumor-derived exosomes mediates STAT3-dependent immunosuppressive function of mouse and human myeloid-derived suppressor cells. J Clin Invest. 2010; 120:457–471. [PubMed: 20093776]

28. Li XQ, Liu JT, Fan LL, Liu Y, Cheng L, Wang F, Yu HQ, Gao J, Wei W, Wang H, Sun GP. Exosomes derived from gefitinib-treated EGFR-mutant lung cancer cells alter cisplatin sensitivity via up-regulating autophagy. Oncotarget. 2016; 7:24585–24595. [PubMed: 27029054]
29. in, National Cancer Institute.
30. Hu G, Chong RA, Yang Q, Wei Y, Blanco MA, Li F, Reiss M, Au JL, Haffy BG, Kang Y. MTDH activation by 8q22 genomic gain promotes chemoresistance and metastasis of poor-prognosis breast cancer. Cancer Cell. 2009; 15:9–20. [PubMed: 19111877]
31. Thery C, Amigorena S, Raposo G, Clayton A. Isolation and characterization of exosomes from cell culture supernatants and biological fluids. Curr Protoc Cell Biol. 2006 Chapter 3. Unit 3 22.
32. Ellman GL, Courtney KD, Andres V Jr, Feather-Stone RM. A new and rapid colorimetric determination of acetylcholinesterase activity. Biochem Pharmacol. 1961; 7:88–95. [PubMed: 13726518]
33. Vichai V, Kirtikara K. Sulforhodamine B colorimetric assay for cytotoxicity screening. Nat Protoc. 2006; 1:1112–1116. [PubMed: 17406391]
34. Au JL, Li D, Gan Y, Gao X, Johnson AL, Johnston J, Millenbaugh NJ, Jang SH, Kuh HJ, Chen CT, Wientjes MG. Pharmacodynamics of immediate and delayed effects of paclitaxel: role of slow apoptosis and intracellular drug retention. Cancer Res. 1998; 58:2141–2148. [PubMed: 9605758]
35. Liang CC, Park AY, Guan JL. In vitro scratch assay: a convenient and inexpensive method for analysis of cell migration in vitro. Nat Protoc. 2007; 2:329–333. [PubMed: 17406593]
36. Geback T, Schulz MM, Koumoutsakos P, Detmar M. TScratch: a novel and simple software tool for automated analysis of monolayer wound healing assays. Biotech. 2009; 46:265–274.
37. Jang SH, Wientjes MG, Au JL. Interdependent effect of P-glycoprotein-mediated drug effux and intracellular drug binding on intracellular paclitaxel pharmacokinetics: application of computational modeling. J Pharmacol Exp Ther. 2003; 304:773–780. [PubMed: 12538833]
38. Jang SH, Wientjes MG, Au JL. Kinetics of P-glycoprotein-mediated efflux of paclitaxel. J Pharmacol Exp Ther. 2001; 298:1236–1242. [PubMed: 11504826]
39. Kuh HJ, Jang SH, Wientjes MG, Au JL. Computational model of intracellular pharmacokinetics of paclitaxel. J Pharmacol Exp Ther. 2000; 293:761–770. [PubMed: 10869374]
40. Venkatasubramanian R, Arenas RB, Henson MA, Forbes NS. Mechanistic modelling of dynamic MRI data predicts that tumour heterogeneity decreases therapeutic response. British journal of cancer. 2010; 103:486–497. [PubMed: 20628390]
41. Williams DP, Shipley R, Ellis MJ, Webb S, Ward J, Gardner I, Creton S. Novel in vitro and mathematical models for the prediction of chemical toxicity. Toxicology research. 2013; 2:40–59. [PubMed: 26966512]
42. Min KA, Zhang X, Yu JY, Rosania GR. Computational approaches to analyse and predict small molecule transport and distribution at cellular and subcellular levels. Biopharm & Drug Dispo. 2014; 35:15–32.
43. Liu C, Krishnan, Xu XY. Towards an integrated systems-based modelling framework for drug transport and its effect on tumour cells. J Bio Eng. 2014; 8:3. [PubMed: 24764492]
44. Wang R, Ding Q, Yaqoob U, de Assuncao TM, Verma VK, Hirsova P, Cao S, Mukhopadhyay D, Huebert RC, Shah VH. Exosome Adherence and Internalization by Hepatic Stellate Cells Triggers Sphingosine 1-Phosphate-dependent Migration. J Bio Chem. 2015; 290:30684–30696. [PubMed: 26534962]
45. Diaz JF, Andreu JM. Assembly of purified GDP-tubulin into microtubules induced by taxol and taxotere: reversibility, ligand stoichiometry, and competition. Biochemistry. 1993; 32:2747–2755. [PubMed: 8096151]
46. Ross JL, Santangelo CD, Makrides V, Fygenson DK. Tau induces cooperative Taxol binding to microtubules. Proc Natl Acad Sci U S A. 2004; 101:12910–12915. [PubMed: 15326286]
47. Ajabnoor GM, Crook T, Coley HM. Paclitaxel resistance is associated with switch from apoptotic to autophagic cell death in MCF-7 breast cancer cells. Cell Death Dis. 2012; 3:e260. [PubMed: 22278287]

48. Caplow M, Shanks J, Ruhlen R. How taxol modulates microtubule disassembly. J Bio Chem. 1994; 269:23399–23402. [PubMed: 7916343]
49. Diaz JF, Strobe R, Engelborghs Y, Souto AA, Andreu JM. Molecular recognition of taxol by microtubules. Kinetics and thermodynamics of binding of fluorescent taxol derivatives to an exposed site. J Bio Chem. 2000; 275:26265–26276. [PubMed: 10818101]
50. Li Y, Edsall R Jr, Jagtap PG, Kingston DG, Bane S. Equilibrium studies of a fluorescent paclitaxel derivative binding to microtubules. Biochem. 2000; 39:616–623. [PubMed: 10642187]
51. Diaz JF, Barasoain I, Andreu JM. Fast kinetics of Taxol binding to microtubules. Effects of solution variables and microtubule-associated proteins. The Journal of biological chemistry. 2003; 278:8407–8419. [PubMed: 12496245]
52. Sutherland RL, Hall RE, Taylor IW. Cell proliferation kinetics of MCF-7 human mammary carcinoma cells in culture and effects of tamoxifen on exponentially growing and plateau-phase cells. Cancer Res. 1983; 43:3998–4006. [PubMed: 6871841]
53. Atay S, Banskota S, Crow J, Sethi G, Rink L, Godwin AK. Oncogenic KIT-containing exosomes increase gastrointestinal stromal tumor cell invasion. Proc Natl Acad Sci U S A. 2014; 111:711–716. [PubMed: 24379393]
54. Kavallaris M. Microtubules and resistance to tubulin-binding agents. Nat Rev Cancer. 2010; 10:194–204. [PubMed: 20147901]
55. Raghunand N, Martinez-Zaguilan R, Wright SH, Gillies RJ. pH and drug resistance. II. Turnover of acidic vesicles and resistance to weakly basic chemotherapeutic drugs. Biochem Pharmacol. 1999; 57:1047–1058. [PubMed: 10796075]
56. Avnet S, Lemma S, Cortini M, Pellegrini P, Perut F, Zini N, Kusuzaki K, Chano T, Grisendi G, Dominici M, De Milito A, Baldini N. Altered pH gradient at the plasma membrane of osteosarcoma cells is a key mechanism of drug resistance. Oncotarget. 2016; 7:63408–63423. [PubMed: 27566564]
57. Federici C, Petrucci F, Caimi S, Cesolini A, Logozzi M, Borghi M, D'Ilio S, Lugini L, Violante N, Azzarito T, Majorani C, Brambilla D, Fais S. Exosome release and low pH belong to a framework of resistance of human melanoma cells to cisplatin. PLoS One. 2014; 9:e88193. [PubMed: 24516610]
58. Shah AK, Wyandt CM, Stodghill SP. Physico chemical characterization of a novel anticancer agent and its comparison to Taxol((R)). Drug Dev Ind Pharm. 2013; 39:89–101. [PubMed: 22339150]
59. Hegmans JP, Bard MP, Hemmes A, Luider TM, Kleijmeer MJ, Prins JB, Zitvogel L, Burgers SA, Hoogsteden HC, Lambrecht BN. Proteomic analysis of exosomes secreted by human mesothelioma cells. American J Patho. 2004; 164:1807–1815.
60. Ribatti D, Marimpietri D, Petretto A, Raffaghello L, Pezzolo A, Gagliani C, Tacchetti C, Mauri P, Melioli G, Pistoia V. Proteome Profiling of Neuroblastoma-Derived Exosomes Reveal the Expression of Proteins Potentially Involved in Tumor Progression. PLoS ONE. 2013; 8:e75054. [PubMed: 24069378]
61. Van de Water L 3rd, Olmsted JB. The quantitation of tubulin in neuroblastoma cells by radioimmunoassay. J Bio Chem. 1980; 255:10744–10751. [PubMed: 7430149]
62. Saari H, Lazaro-Ibanez E, Viitala T, Vuorimaa-Laukkanen E, Siljander P, Yliperttula M. Microvesicle-and exosome-mediated drug delivery enhances the cytotoxicity of Paclitaxel in autologous prostate cancer cells. J Control Release. 2015; 220:727–737. [PubMed: 26390807]
63. Kim MS, Haney MJ, Zhao Y, Mahajan V, Deygen I, Klyachko NL, Inskoe E, Piroyan A, Sokolsky M, Okolie O, Hingtgen SD, Kabanov AV, Batrakova EV. Development of exosome-encapsulated paclitaxel to overcome MDR in cancer cells. Nanomedicine. 2016; 12:655–664. [PubMed: 26586551]

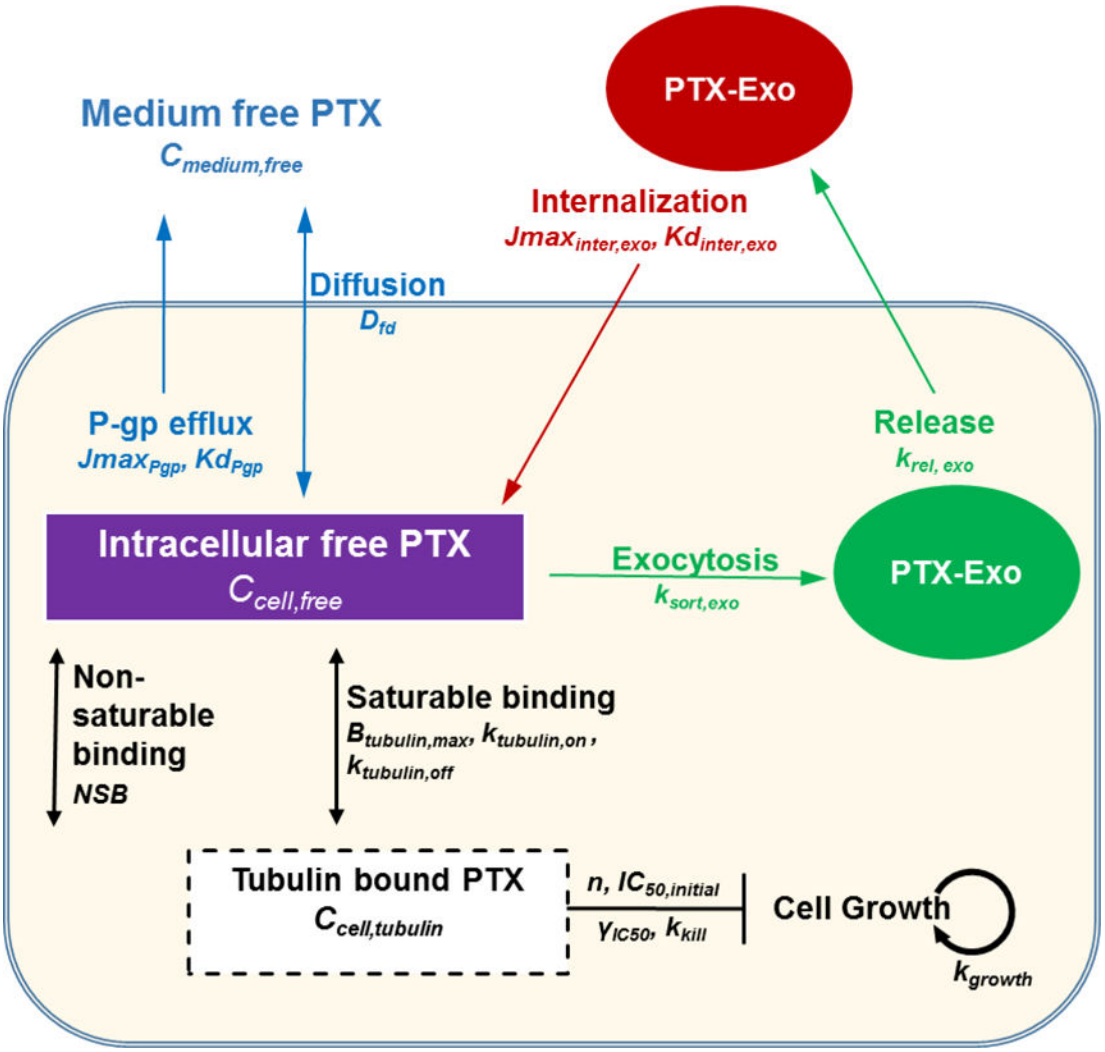

Figure 1. Cellular pharmacokinetic/pharmacodynamic models of paclitaxel

$C_{medium,free}$ or $C_{cell,free}$ is free (unbound) drug concentration in medium or cells, respectively. $C_{cell,tubulin}$ is the tubulin-bound drug concentration. D_{fd} is the rate constant of passive diffusion of free drug. $Jmax_{Pgp}$ is the maximum Pgp-mediated drug efflux rate. Kd_{Pgp} is the dissociation constant of drug from Pgp. $C_{medium,exo}$ or $C_{cell,exo}$ is the drug concentration in extracellular or intracellular exosomes, respectively. $Jmax_{inter,exo}$ is the maximum rate of receptor-mediated internalization of exosomes. $Kd_{inter,exo}$ is the dissociation constant of exosome from receptor for internalization. $k_{sort,exo}$ is the rate constant of drug sorting into exosomes. $k_{rel,exo}$ is the rate constant of exosome release into extracellular space. $B_{tubulin,max}$ is the maximum available drug binding sites in tubulin. $k_{tubulin,on}$ or $k_{tubulin,off}$ are the rate constants of drug association and disassociation with tubulin, respectively. NSB is the proportion constant for the linear nonsaturable drug binding in cells. For PD parameters, IC_{50} is the tubulin-bound drug concentration needed to generate 50% of maximum drug effect, k_{kni} is the maximal rate constant of cell kill. n is Hill exponent.

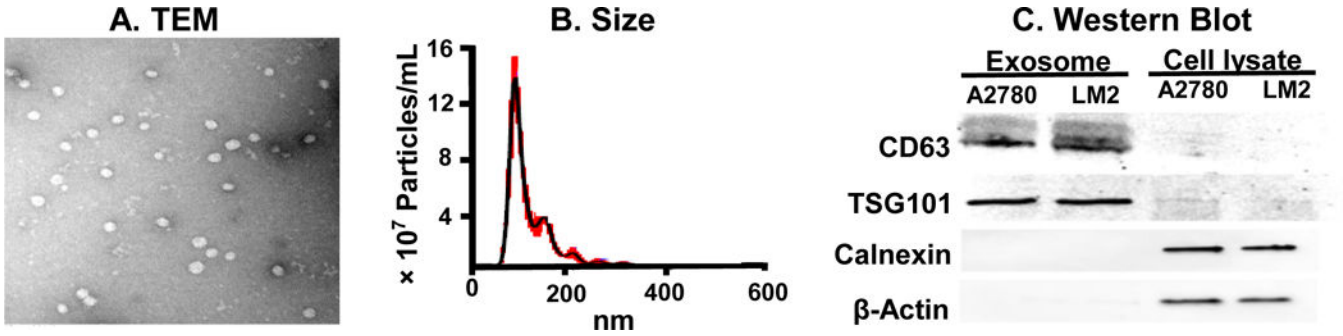

Figure 2. Characterization of cancer cell-derived exosomes

(A) Transmission electron microscopy. Representative image of MCF7 exosomes. (B) Size distribution of MCF7 exosomes by nanoparticle tracking analysis. Black: rolling average. Red: SD of results from three repeated measurements. (C) Western blot results. Exosomes and Donor cell lysates, collected from A2780 cells and LM2 cells, were analyzed for CD63, TSG101, calnexin and β-actin.

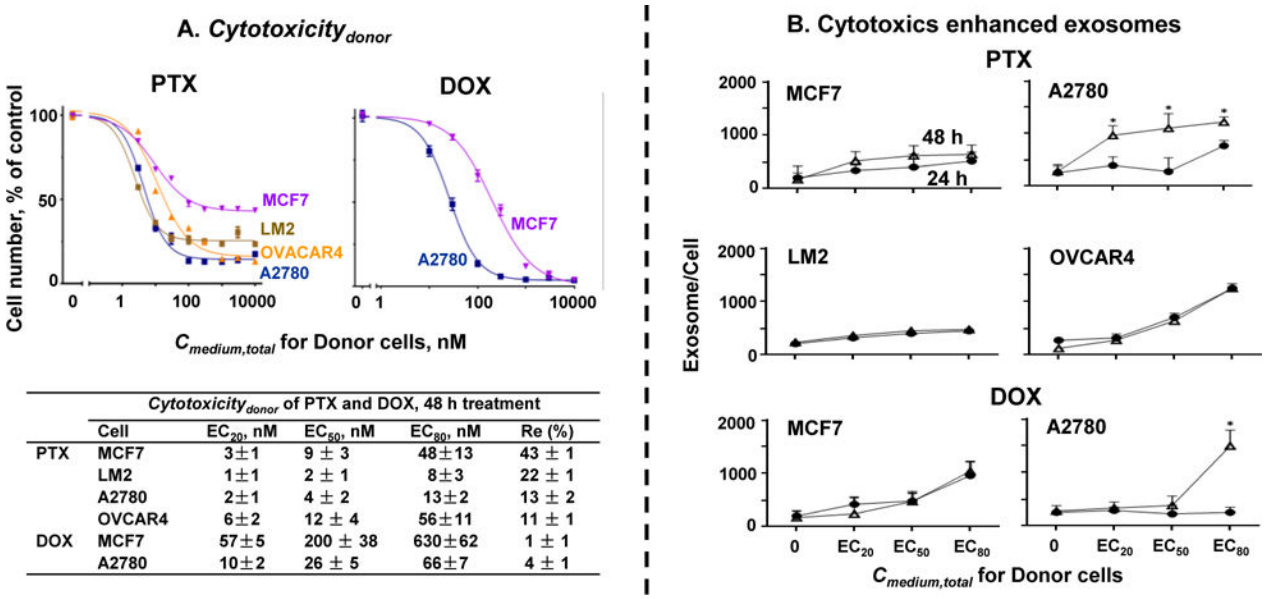

	Cytotoxicity donor of PTX and DOX, 48 h treatment				
	Cell	EC_{20}, nM	EC_{50}, nM	EC_{80}, nM	Re (%)
PTX	MCF7	3±1	9 ± 3	48±13	43 ± 1
	LM2	1±1	2 ± 1	8±3	22 ± 1
	A2780	2±1	4 ± 2	13±2	13 ± 2
	OVCAR4	6±2	12 ± 4	56±11	11 ± 1
DOX	MCF7	57±5	200 ± 38	630±62	1 ± 1
	A2780	10±2	26 ± 5	66±7	4 ± 1

Figure 3. Cytotoxic concentrations of paclitaxel and doxorubicin induced exosome production and/or release

(A) *Cytotoxicity*$_{donor}$ of PTX and DOX. MCF7, LM2, A2780, and OVCAR4 cells were treated for 24 or 48 h with PTX or DOX, and the remaining cell numbers were determined using SRB assay. Results were analyzed for the values of drug concentrations producing 20%, 50% and 80% of the maximal cytotoxicity (EC_{20}, EC_{50} and EC_{80}, respectively). (B) Cytotoxics enhanced exosomes. Cells were treated for 24 h or 48 h with PTX or DOX at $C_{medium,total}$ equivalent to their EC_{20}, EC_{50} and EC_{80} for 48 h treatment. Number of exosomes in culture medium after drug treatment for 24 h (circles) and 48 h (open triangles) were standardized by cell numbers (mean ± SE, n = 3 experiments, four replicates per experiment). *p<0.01 for 24 h *vs.* 48 h (unpaired Student's t-test).

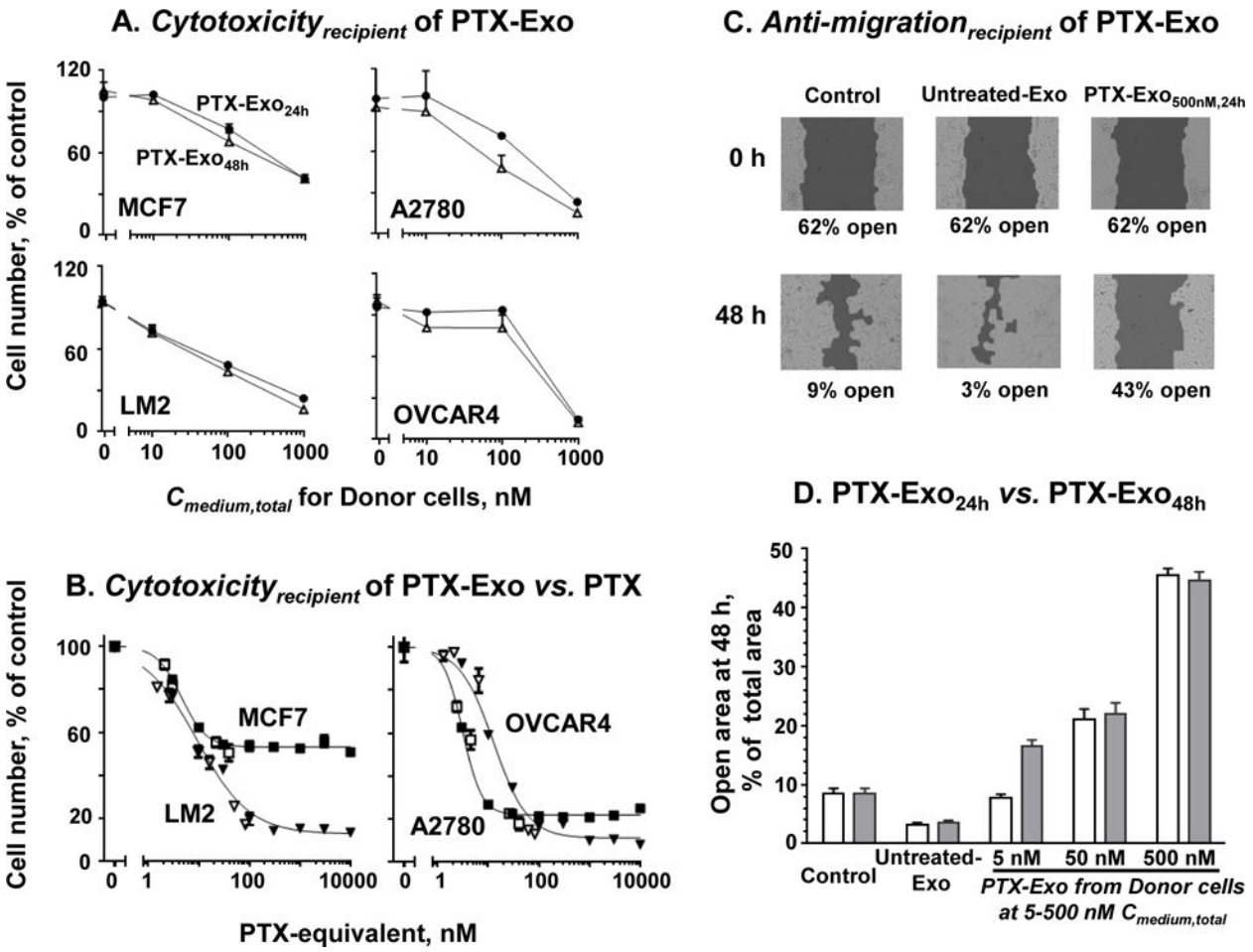

Figure 4. PTX-Exo conferred dose-dependent *Cytotoxicity*$_{recipient}$ (A and B) and *Anti-migration*$_{recipient}$ (C and D)

For (A) and (B), drug-naïve cells (MCF7, LM2, A2780, OVCAR4) were treated with PTX or PTX-Exo collected from Conditioned Medium of their corresponding Donor cells. The Recipient cell number was determined using SRB assay. Data are Mean ± SD (n=4 experiments with triplicates per experiment). (A) *Cytotoxicity*$_{recipient}$ of PTX-Exo. PTX-Exo$_{24h}$ (circles) and PTX-Exo$_{48h}$ (open triangles), both containing 10 μg proteins, were incubated with Recipient cells for 48 h. (B) Comparison of *Cytotoxicity*$_{recipient}$ of PTX-Exo and PTX. Recipient cells were treated with PTX (solid symbols) or PTX-Exo (open symbols) collected from Donor cells after 24 h PTX treatment. The x-axis denotes the PTX-equivalent concentration added to the culture medium, where the amount of the added PTX-Exo was calculated based on the LC-MS/MS results. Note the different scales in (A) and (B). For (C) and (D), LM2 cells were cultured in 6-well plates, without drug treatment (control), or treatment with exosomes collected from untreated Donor cells (Untreated Exo) or PTX-Exo for 48 h. The exosomes added to each well contained 100 μg proteins. (C) Inhibition of cell migration. The initial open areas (i.e., not covered by cells) in untreated control and Untreated-Exo groups were equal (62 ± 2%; mean ± SD, n=6 experiments, duplicates in each experiment). (D) Concentration- and time-dependent *Anti-migration*$_{recipient}$ by PTX-Exo$_{24h}$ (open bars) and PTX-Exo$_{48h}$ (filled bars) harvested from

Donor cells treated with 5, 50 or 500 nM PTX. Statistically significant differences between (a) Control and other groups ($p<0.01$, Dunnett's test), (b) Untreated-Exo and PTX-Exo groups ($p<0.01$, Dunnett's test), (c) among the three PTX-Exo groups at different $C_{medium,total}$ ($p<0.01$, Dunnett's test), and (d) between PTX-$Exo_{5nM,24h}$ and PTX-$Exo_{5nM,48h}$ (*$p<0.01$, unpaired Student's t-test).

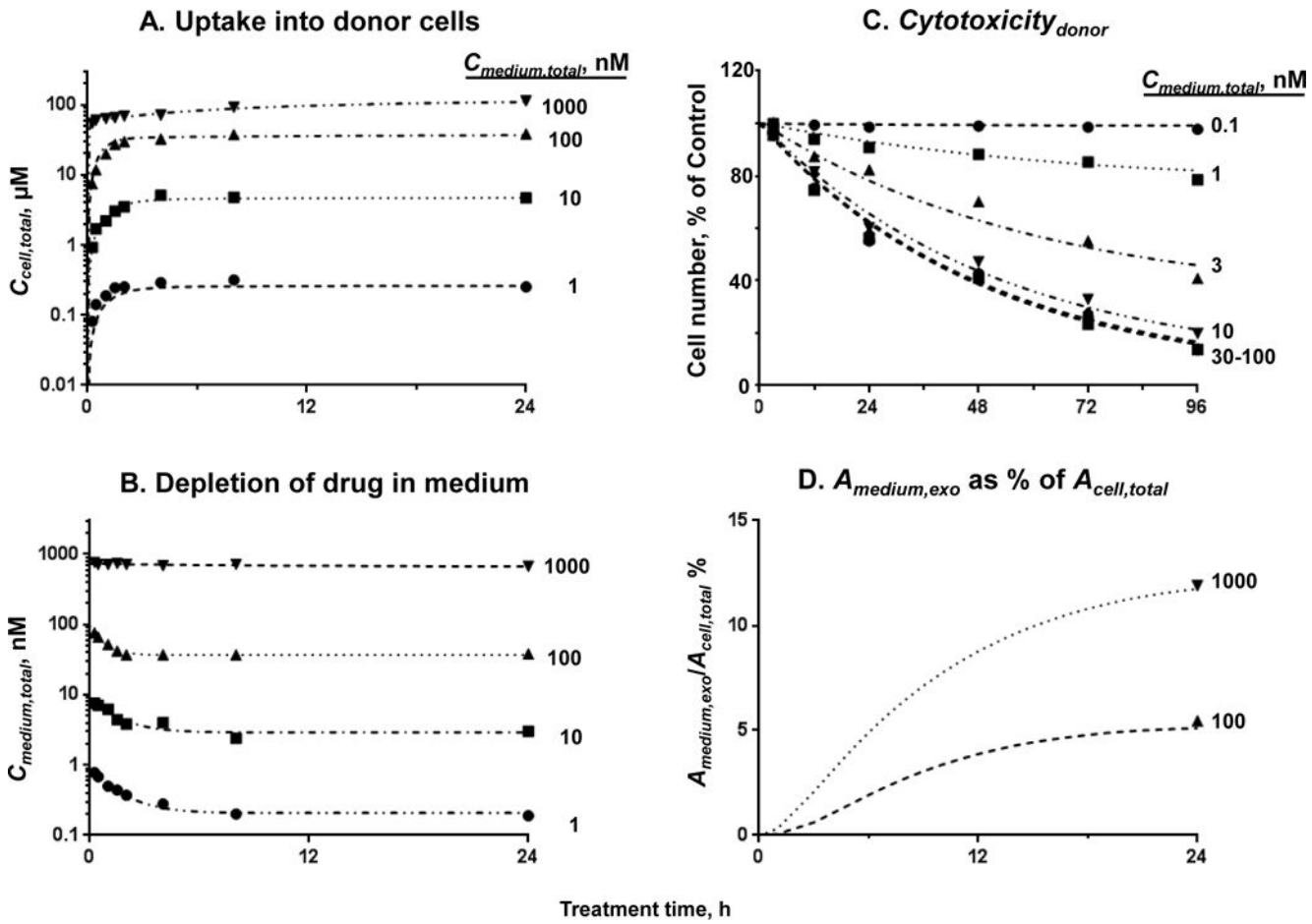

Figure 5. Obtaining model parameters

(A) Donor cell $C_{cell,total}$ *vs.* time plots. (B) Time-dependent changes in $C_{medium,\ total}$ at four initial $C_{medium,total}$ (1 to 1000 nM). (C) $Cytotoxicity_{donor}$ *vs.* treatment concentration and duration plots. (D) Changes of $A_{medium,exo}$ as a fraction of $A_{cell,total}$ in Donor cells with time. The experimental results in (A), (B) and (C) were from our earlier studies ([34, 39] with permission), and the results in (D) are from the current study (calculated from Table 1; 24 h results only). Fitting Eq. 1–13 to the experiment data points (symbols) yielded the best-fitting curves and model parameter values (see text). Note the different x and y scales (i.e., 24 h in (A), (B) and (D) *vs.* 96 h in (C); logarithmic in (A) and (B) *vs.* linear in (C) and (D)).

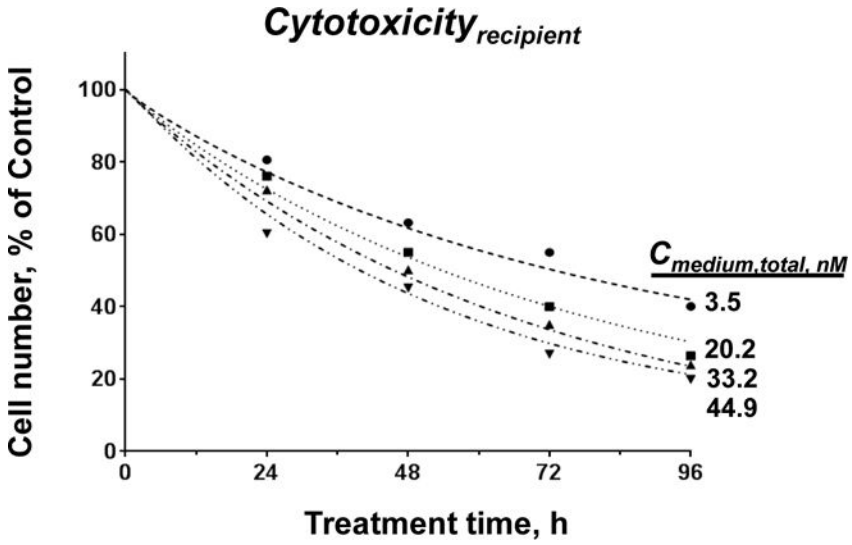

Figure 6. QP model-simulated pharmacodynamics of PTX-Exo: Comparison with experimental results

Model-simulated results (curves) *vs.* experimentally observed results (symbols) on $Cytotoxicity_{recieint}$ of PTX-Exo as functions of drug treatment concentration and duration. Drug concentrations in culture medium at time zero were calculated as [drug amount in PTX-Exo] divided by extracellular fluid volume (equaled 1000 μL). For experimental data, the remaining cell number was measured using SRB assay (n = 3 experiments, four replicates per experiment). Deviations between simulated and experimental results were 12 ± 7% (mean ± SD).

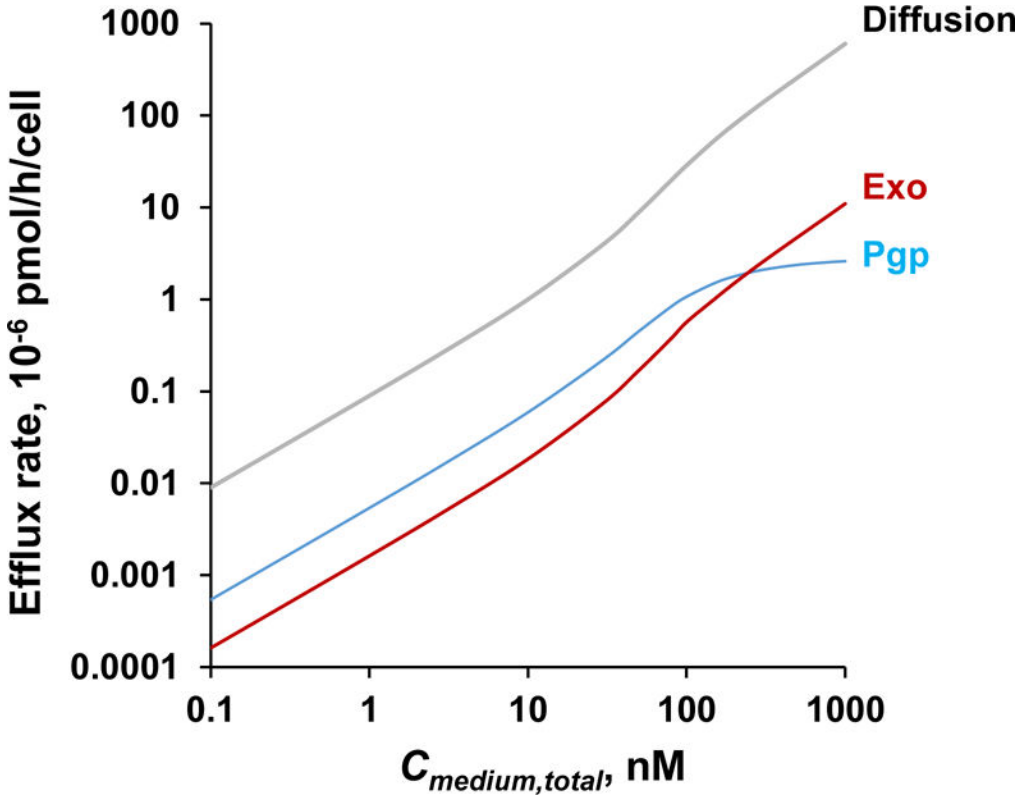

Figure 7. Contribution of drug efflux mechanisms

Drug efflux rates by passive diffusion and two active efflux mechanisms (Pgp and exosomes) were simulated using Eq. 3–4 for cells treated with 0.1–1000 nM PTX for 24 h.

J Control Release. Author manuscript; available in PMC 2018 December 28.

Table 1

Amount of PTX in PTX-Exo or cell lysates

Cells were treated with 100 or 1000 nM PTX for 24 h. PTX-Exo was collected from Conditioned Medium. Cells were washed and collected with trypsinization, counted and lyzed. Drug concentrations in exosomes and cell lysates were analyzed using LC-MS/MS, and standardized to cell number. The numbers of exosomes per LM2, MCF7, A2780 and OVCAR4 cell were, respectively, 1170, 955, 2236 and 2457 at 100 nM PTX and 1232, 1060, 2513 and 2794 at 1000 nM PTX. Results are mean ± SD (three independent experiments with three replicates per experiment).

Cell line	PTX, pmole per 10^6 Donor cells					
	Treated with 100 nM PTX			Treated with 1000 nM PTX		
	Exosome	Lysate	Exosome-to-Lysate ratio, %	Exosome	Lysate	Exosome-to-Lysate ratio %
LM2	1.13±0.02	25.0±0.10	4.27±0.22	6.18±0.65	62.2±0.19	9.29 ± 1.08
MCF7	1.60±0.04	29.3±0.54	5.12±0.36	8.33±0.16	69.7±0.53	11.59 ± 0.79
A2780	1.44±0.08	23.8±0.23	6.67±1.12	5.38±0.27	73.4±3.49	7.67 ± 1.64
OVCAR4	2.38±0.06	28.6±0.47	8.28±0.69	6.71±0.46	71.7±2.72	9.65 ± 0.33
Average	1.64±0.27	26.7±1.34	6.08±1.77	6.65±0.62	69.3±2.46	9.55 ± 1.61

Table 2
PTX cellular pharmacokinetic and pharmacodynamic model parameters

Some parameter values were obtained from the literature and some were obtained from analyzing the experimental results of the current study (indicated as Analysis). Mean values of parameters obtained from Analysis are shown with % CV in parentheses.

Category	Parameter	Annotation	Value (% CV)	Source
A. Cellular pharmacokinetic model				
Pgp-mediated efflux	$Jmax_{Pgp}$ (pmoleh^{-1}·cell^{-1})	Maximum Pgp efflux rate	2.8×10^{-6}	[37]
	Kd_{Pgp} (nM)	Dissociation constant of drug from Pgp	13.9	[37]
Diffusion	D_{fd} (μL·h^{-1}·cell^{-1})	Diffusion rate constant of free PTX across cell membrane	3.34×10^{-3}	[39]
Intracellular microtubule binding	$B_{tubulin,initial}$ (μM)	Maximal initial PTX binding sites on tubulin	59.2	[39]
	$k_{tubulin,off}$ (s^{-1})	Rate constant of PTX dissociation from tubulin	30	[48]
	$k_{tubulin,on}$ (nM^{-1}·s^{-1})	Rate constant of PTX association with tubulin	2	[48]
Binding to cell or extracellular fluid	$B_{medium,max}$ (μM)	Maximal extracellular drug binding sites	3.94	[39]
	$Kd_{medium,bound}$ (nM)	Dissociation constant of PTX from extracellular binding sites	781	[39]
	V_{cell} (μL)	Volume of single cell	2.06×10^{-6}	[39]
	Vm (μL)	Medium volume	1000	Experimental set-up
Exosome release and internalization	$Jmax_{inter,exo}$ (pmole·h^{-1}·cell^{-1})	Maximum rate of endocytosis of extracellular exosomes	0.038 (23)	Analysis
	$Kd_{inter,exo}$ (nM)	Dissociation constant of exosomes from endocytosis receptor	63 (45)	Analysis
	$k_{sort,exo}$ (h^{-1})	Rate constant for sorting intracellular PTX into exosome	31 (67)	Analysis
	$k_{rel,exo}$ (h^{-1})	Rate constant for exosomes release into extracellular fluid	0.105 (12)	Analysis
B. Pharmacodynamic model				
Drug cytotoxicity	k_{growth} (h^{-1})	Cell growth rate constant	0.0288 (8)	Analysis
	k_{kill} (h^{-1})	Maximum cell kill rate constant	0.0202 (11)	Analysis
	$IC_{50,initial}$ (nM)	Tubulin-bound concentration to produce 50% E_{max} at time zero	826 (27)	Analysis
	γ_{IC50} (nM·h^{-1})	Change in IC_{50} over treatment time	7.2 (48)	Analysis

Category	Parameter	Annotation	Value (% CV)	Source
	n	Hill exponent of PTX concentration-cytotoxicity curve	1.67 (4)	Analysis
	Nss	Maximum cell number at confluence	1.1×10^6	Experimentally determined
	ICN	Initial cell number	5×10^3	Experimental set-up

Table 3

Effect of exosome production and internalization on PTX accumulation and cytotoxicity in cells: Model-simulated results

Simulations were performed for Donor cells treated with 1 or 1000 nM PTX for 24 h. The resulting values of $C_{cell,total}$, $C_{cell,tubulin}$ and *Cytotoxicity* (*E*, rate constant of drug-induced cell death) are represented as area-under-curve from 0 to 24 h. *E* was calculated as $k_{kill} \cdot \left(\frac{{C_{cell,tubulin}}^{n}}{{C_{cell,tubulin}}^{n} + IC_{50}^{n}} \right)$. The original values of model parameters are 31 h^{-1} for $k_{sort,exo}$, 0.105 h^{-1} for $k_{rel,exo}$, 0.038 pmole·h^{-1}·$cell^{-1}$ for $Jmax_{inter,exo}$, and 59.2 μM for $B_{tubulin,initial}$. With the exception of $B_{tubulin,initial}$ where the low and high values were one-half or 2-times the original values, the low and high values of all other parameters were one-tenth or 10-times the original values. Signs in the table correspond to minimal change of <20% (−), increase or decrease of 20–50% (↑ and ↓), 51–100% (↑↑ and ↓↓), 101–200% (↑↑↑ and ↓↓↓), and >200% (↑↑↑↑ and ↓↓↓↓).

Parameter			A. Effects on Donor cells						B. Effects on Recipient cells				
			1 nM			1000 nM			1 nM			1000 nM	
$C_{cell,total}$	$C_{cell,tubulin}$	E	$C_{cell,total}$	$C_{cell,tubulin}$	E	$C_{cell,total}$	$C_{cell,tubulin}$	E	$C_{cell,total}$	$C_{cell,tubulin}$	E		
Exosome production	$k_{sort,exo}$	Low	–	–	–	↑	–	–	↓	↓	↓↓	↓	↓	↓↓
		High	–	–	–	↓	–	–	↑	↑	↑↑	↑↑	↑↑	↑↑
	$k_{rel,exo}$	Low	↑	↑↑	↑↑ ↑↑	↑	↑	–	↓	↓	↓↓	↓↓	↓↓	↓↓↓
		High	↓	↓↓	↓↓ ↓↓	↓	↓	–	↑↑	↑↑	↑↑ ↑	↑↑	↑↑	↑↑↑ ↑
Exosome internalization	$Jmax_{inter,exo}$	Low	–	↓	↓	–	–	–	↑	↑	↑↑ ↑	↑↑	↑↑	↑↑↑ ↑
		High	–	↑	↑	–	–	–	↓	↓	↓	↓	↓	↓↓
Tubulin binding capacity	$B_{tubulin,initial}$	Low	↓	↓↓	↓↓ ↓	↓↓	↓↓↓	–	↑	↑	↑	↑	↑↑	↑↑
		High	↑	↑↑	↑↑ ↑	↑↑	↑↑↑	–	↓	↓	↓↓	↓	↓	↓↓

J Control Release. Author manuscript; available in PMC 2018 December 28.